View metadata, citation and similar papers at core.ac.uk

brought to you by CORE

provided by DigitalCommons@University of Nebraska

University of Nebraska - Lincoln

DigitalCommons@University of Nebraska - Lincoln

US Department of Energy Publications

U.S. Department of Energy

2011

The mineralogic transformation of ferrihydrite induced by heterogeneous reaction with bioreduced anthraquinone disulfonate (AQDS) and the role of phosphate

John M. Zachara
Pacific Northwest National Laboratory, john.zachara@pnl.gov

Ravi K. Kukkadapu
Pacific Northwest National Laboratory, ravi.kukkadapu@pnl.gov

Tanya Peretyazhko
Pacific Northwest National Laboratory

Mark Bowden
Pacific Northwest National Laboratory

Chongmin Wang
Pacific Northwest National Laboratory

See next page for additional authors

Follow this and additional works at: https://digitalcommons.unl.edu/usdoepub

 Part of the Bioresource and Agricultural Engineering Commons

Zachara, John M.; Kukkadapu, Ravi K.; Peretyazhko, Tanya; Bowden, Mark; Wang, Chongmin; Kennedy, David; Moore, Dean; and Arey, Bruce, "The mineralogic transformation of ferrihydrite induced by heterogeneous reaction with bioreduced anthraquinone disulfonate (AQDS) and the role of phosphate" (2011). *US Department of Energy Publications*. 263.
https://digitalcommons.unl.edu/usdoepub/263

This Article is brought to you for free and open access by the U.S. Department of Energy at DigitalCommons@University of Nebraska - Lincoln. It has been accepted for inclusion in US Department of Energy Publications by an authorized administrator of DigitalCommons@University of Nebraska - Lincoln.

Authors

John M. Zachara, Ravi K. Kukkadapu, Tanya Peretyazhko, Mark Bowden, Chongmin Wang, David Kennedy, Dean Moore, and Bruce Arey

This article is available at DigitalCommons@University of Nebraska - Lincoln: https://digitalcommons.unl.edu/usdoepub/263

Available online at www.sciencedirect.com

SciVerse ScienceDirect

Geochimica et Cosmochimica Acta 75 (2011) 6330–6349

Geochimica et Cosmochimica Acta

www.elsevier.com/locate/gca

The mineralogic transformation of ferrihydrite induced by heterogeneous reaction with bioreduced anthraquinone disulfonate (AQDS) and the role of phosphate

John M. Zachara *, Ravi K. Kukkadapu, Tanya Peretyazhko, Mark Bowden, Chongmin Wang, Dave W. Kennedy, Dean Moore, Bruce Arey

Pacific Northwest National Laboratory, P.O. Box 999, MSIN K8-96, Richland, WA 99354, USA

Received 4 November 2010; accepted in revised form 27 April 2011; available online 29 June 2011

Abstract

Bioreduced anthraquinone-2,6-disulfonate (AH_2DS; dihydro-anthraquinone) was reacted with a 2-line, Si-substituted ferrihydrite under anoxic conditions at neutral pH in PIPES buffer. Phosphate (P) and bicarbonate (C); common adsorptive oxyanions and media/buffer components known to effect ferrihydrite mineralization; and $Fe(II)_{aq}$ (as a catalytic mineralization agent) were used in comparative experiments. Heterogeneous AH_2DS oxidation coupled with Fe(III) reduction occurred within 0.13–1 day, with mineralogic transformation occurring thereafter. The product suite included lepidocrocite, goethite, and/or magnetite, with proportions varing with reductant:oxidant ratio (r:o) and the presence of P or C. Lepidocrocite was the primary product at low r:o in the absence of P or C, with evidence for multiple formation pathways. Phosphate inhibited reductive recrystallization, while C promoted goethite formation. Stoichiometric magnetite was the sole product at higher r:o in the absence and presence of P. Lepidocrocite was the primary mineralization product in the $Fe(II)_{aq}$ system, with magnetite observed at near equal amounts when Fe(II) was high [Fe(II)/Fe(III)] = 0.5 and P was absent. P had a greater effect on reductive mineralization in the $Fe(II)_{aq}$ system, while AQDS was more effective than $Fe(II)_{aq}$ in promoting magnetite formation. The mineral products of the direct AH_2DS-driven reductive reaction are different from those observed in AH_2DS-ferrihydite systems with metal reducing bacteria, particularly in presence of P.
© 2011 Elsevier Ltd. All rights reserved.

1. INTRODUCTION

Dissimilatory Fe(III) reduction under anoxic geochemical conditions is an important biogeochemical process in soils, sediments, and subsurface systems mediated by metal reducing bacteria (MRB). The process has been extensively studied (Geomicrobiology, 2002; DiChristina et al., 2005; Kappler and Straub, 2005; Roden, 2006; Weber et al., 2006). Dissimilatory Fe(III) reduction influences system redox state and buffering capacity (Fredrickson et al., 2004; Komlos et al., 2007); the valence and composition of pore-water solutes (Baedecker et al., 1993; Bennett et al., 1993); the identity, surface properties, and geochemical reactivity of the Fe-containing mineral fraction (e.g., Zachara et al., 2004; Plymale et al., 2011); and the chemical form, persistence, and fate of a wide range of inorganic and organic contaminants (Lovley and Anderson, 2000).

MRB access Fe(III) in mineral forms by direct cellular contact (Nevin and Lovley, 2000a; Mehta et al., 2005; Shi et al., 2007), dissolution-promoting Fe(III) chelators (Taillefert et al., 2007; Jones et al., 2010), and water soluble endogenous or exogenous electron transfer mediators (ETM; Nevin and Lovley, 2000b; Straub and Schink, 2003; Marsili et al., 2008; O'Loughlin, 2008). The dissimilatory reduction of numerous Fe(III)-containing subsurface

* Corresponding author. Tel.: +1 509 371 6355; fax: +1 509 371 6354.

E-mail address: john.zachara@pnl.gov (J.M. Zachara).

0016-7037/$ - see front matter © 2011 Elsevier Ltd. All rights reserved.
doi:10.1016/j.gca.2011.06.030

This article is a U.S. government work, and is not subject to copyright in the United States.

mineral forms have been studied, with recognition that high surface area and high solubility are conducive to bioreduction because of surface chemical and thermodynamic constraints (Roden and Zachara, 1996; Bonneville et al., 2004; Roden, 2006; Yan et al., 2008). The following bioavailability sequence has been observed based on total Fe(III) mass: ferrihydrite ~ lepidocrocite > nanocrystalline Fe(III) oxides > Fe(III) containing phyllosilicates (smectite, nontronite, illite) > crystalline Fe(III) oxides (Roden and Zachara, 1996; Kostka et al., 2002; Zachara et al., 2002; Bonneville et al., 2004). The bioreduction of ferrihydrite and lepidocrocite, specifically, can lead to major changes in mineralogy (Fredrickson et al., 1998; Hansel et al., 2003; Kukkadapu et al., 2004, 2005; O'Loughlin et al., 2007).

The addition of the synthetic ETM, 9,10-anthraquinone-2,6-disulfonate (AQDS), to an anoxic MRB–Fe(III) mineral suspension with a suitable electron donor greatly enhances the Fe(III) reduction rate and extent (Fredrickson et al., 1998; Zachara et al., 1998; Royer et al., 2002; Dong et al., 2003; Hernandez et al., 2004; Chacon et al., 2006; Kukkadapu et al., 2006; Behrends and van Cappellen, 2007; Jaisi et al., 2007; Coker et al., 2008; Cutting et al., 2009). AQDS is a widely used model ETM for environmental and contaminant redox transformations of diverse type (Curtis and Reinhard, 1994; Borch et al., 2005; Bhushan et al., 2006; Kwon and Finneran, 2006, 2008; Zhang et al., 2007). AQDS is a synthetic three-ring quinone with structural analogy to quinone groups in humic substances (Curtis and Reinhard, 1994), and to biogenic quinones (Nurmi and Tratnyek, 2002). AQDS has a relatively low half-cell potential, and rapid redox kinetics (Nurmi and Tratnyek, 2002). It readily engages with the electron transport system of certain MRB (Shyu et al., 2002; Voordeckers et al., 2010), being reduced to the dihydroanthraquinone state (AH_2DS):

$$AQDS + 2H^+ + 2e^- = H_2DS \quad E^o = 0.23V$$

The AH_2DS form is poorly adsorbed, but rapidly reactive with Fe(III) oxides (Liu et al., 2007a). The product of the heterogeneous AH_2DS reaction with Fe(III) mineral phases is Fe(II) in either a structural or adsorbed state that has not been well characterized.

Numerous studies of ferrihydrite or lepidocrocite reductive biomineralization by MRB have used AQDS as a mediator, observing that its presence yields more crystalline mineralogic products (e.g., Fredrickson et al., 1998; Zachara et al., 1998). Reductive mineral phases have been observed in AQDS-containing Fe(III) oxide systems, such as green rust and ferrous hydroxy carbonate (Ona-Nguema et al., 2002; Kukkadapu et al., 2004, 2005; O'Loughlin et al., 2007; O'Loughlin, 2008), that are infrequently observed in its absence. These mineral forms are considered biomineralization products, but are they? Unclear is whether noted mineralogic differences between AQDS (±)–ferrihydrite/lepidocrocite–MRB systems result from the heterogeneous reaction pathways of AH_2DS; unique biogenic kinetic flux rates of AH_2DS, Fe(II), or HCO_3^- (resulting from electron donor oxidation); or changes in bacteria-mineral biophysical interaction, aggregation, and the consequent interfacial microenvironment. Some believe that AQDS has no direct influence or control on the nature of bioreductive mineral products other than a kinetic one (Zegeye et al., 2007; Coker et al., 2008).

As a first step in understanding the AQDS–ferrihydrite/lepidocrocite–MRB system, we investigated mineral transformations promoted by interaction of bioreduced AQDS with a Si-containing, 2-line ferrihydrite. We varied the AH_2DS/Fe(III) ratio and investigated the effects of phosphate (PO_4^{3-}) and bicarbonate (HCO_3^-), ubiquitous natural ligands and common components of bacterial incubation media, on reductive mineral transformation. Resultant mineral products were characterized by scanning and transmission electron microscopy, X-ray diffraction, and variable temperature Mössbauer spectroscopy. The mineralization promoting effects of AH_2DS were compared to those of $Fe(II)_{(aq)}$, and the results of Hansel et al. (2005) and Borch et al. (2007), who studied similar Fe(II) systems.

2. MATERIALS AND METHODS

2.1. Two-line 0.02 Si-ferrihydrite

Two-line ferrihydrite containing 2% Si [Si/(Si + Fe) mole fraction = 0.02] was prepared using ferric nitrate (0.333 mol L^{-1}) and sodium meta-silicate (0.012 mol L^{-1}) solutions (Kukkadapu et al., 2004). Silica was co-precipitated with ferrihydrite to retard the progress of oxidative recrystallization reactions (e.g., to 6-line ferrihydrite, goethite, and hematite) that proceed relatively rapidly in its absence (Anderson and Benjamin, 1985; Kukkadapu et al., 2003; Dyer et al., 2010). The resulting ferrihydrite suspension was washed with 1.0×10^{-4} mol L^{-1} $NaClO_4$ to remove nitrate and dissolved Si, and (1) stored as $\sim 5.0 \times 10^{-1}$ mol L^{-1} Fe suspension (pH 7.0) in 1.0×10^{-4} mol L^{-1} $NaClO_4$ at 4 °C [for AH_2DS experiments (Section 3.1)], or (2) manipulated to yield 1.0×10^{-2} mol L^{-1} ferrihydrite in 1.0×10^{-2} mol L^{-1} anoxic PIPES buffer at pH 7 [for Fe(II) experiments (Section 3.2)]. The Si-ferrihydrite was recrystallization stable for months in suspensions that are saturated with atmospheric oxygen.

2.2. Bioreduced AQDS (AH_2DS)

AQDS was incubated with *Shewanella oneidensis* strain MR-1 in presence of H_2 (electron donor) to yield AH_2DS (Liu et al., 2007a). The method involved incubation at 30 °C and 150 rpm of 160 mL serum bottles containing 90 mL of AQDS, 30 mL H_2, and 10 mL washed cells in 3.0×10^{-2} mol L^{-1} anaerobic buffer [PIPES (head space O_2-free N_2)]. This composition corresponded to 2×10^8 cells mL^{-1} and 5.0×10^{-3} mol L^{-1} AQDS. The bottles were incubated until a color change (4–6 d) indicated conversion of AQDS to AH_2DS. Complete reduction of AQDS to AH_2DS was confirmed by UV–VIS spectroscopy (Liu et al., 2007a). The AH_2DS solution was anaerobically filtered (0.2 μm) into a sterile serum vial to remove cell fragments, and tightly sealed.

Bacterial reduction of AQDS to AH_2DS was selected because it was representative of the MRB–AQDS system that we sought to understand. Additionally, it was more effective than abiotic synthesis, yielding >98% AH_2DS solutions. It is possible that other redox-active biomolecules may have been secreted to solution during AH_2DS synthesis, although these are likely to be low in concentration in the absence of a carbon source. Potential candidates include riboflavin and riboflavin 5′-phosphate, compounds suspected to be electron transfer mediators (Marsili et al., 2008). Direct analyses of *S. oneidensis* MR-1 cultures, the organism used here for AQDS reduction, place FMN and riboflavin at nominal concentrations of 250–500 nM (Marsili et al., 2008), or <0.01% of the total AH_2DS concentration. Reductive dissolution experiments performed in our laboratory with these compounds and 2-line ferrihydrite indicate that these low flavin concentrations did not influence the outcome of the experiments reported herein because of the large excess of AH_2DS.

2.3. Reductive transformation of 2-line Si-ferrihydrite with AH_2DS

AH_2DS concentrations were chosen to yield two $Fe(II)_{equiv}/Fe(III)$ ratios (0.11, 0.54; where $Fe(II)_{equiv}/Fe(III) = 2[AH_2DS]/(Fe(III)_{initial} - 2[AH_2DS])$ after its heterogeneous oxidation by ferrihydrite (Table 1). The lower ratio is slightly below the threshold value (0.124) reported by Hansel et al. (2005) for magnetite formation, while the higher value (0.54) is approximately equal to the Fe(II)/Fe(III) ratio in magnetite (0.5). Ferrihydrite in 3.0×10^{-2} mol L^{-1} PIPES buffer (100 mL; pH 7; O_2-free N_2 head space), untreated or pretreated (overnight) with PO_4^{3-} (P) and/or HCO_3^- (C), was incubated with the two AH_2DS concentrations for 0.13, 1, and 30 d. These incubation times were chosen based on a scoping experiment that identified the time period of transformation. The AH_2DS, P, and C concentrations; and AH_2DS/Fe, $Fe(II)_{equiv}/Fe(III)$, $P/(Fe + P)$, and $C/(Fe + C)$ ratios of the experiments are summarized in Table 1. The incubations were carried out in 160 mL serum bottles with butyl rubber stoppers and Al crimp-seals at 30 °C and 25 rpm horizontal shaking. The C concentrations (0.25 and 0.75×10^{-3} mol L^{-1} as HCO_3^-) are typical of groundwater, and those found as an electron donor oxidation product in MRB–Fe(III) oxide suspensions (Fredrickson et al., 1998). The P concentration (0.6×10^{-3} mol L^{-1}) falls at the low end of that used in MRB laboratory studies.

2.4. Treatment of 2-line Si-ferrihydrite with aqueous Fe(II)

Aqueous ferrous iron concentrations of 0.5, 3.3, and 5.0×10^{-3} mol L^{-1} were selected to bracket the $Fe(II)_{equiv}/Fe(III)$ ratio of 0.11 used in the AH_2DS experiment at the low end, and to approximate the ratio of 0.54 at the high end. Approximately 17.5 mL of 2-line Si-ferrihydrite (2.0×10^{-2} mol L^{-1}) in 1.0×10^{-3} mol L^{-1} PIPES buffer (pH 7; O_2-free N_2 head space), untreated or pretreated overnight with 2% P, was contacted with the three concentrations of $Fe(ClO_4)_2$ (in 17.5 mL of 1.0×10^{-2} mol L^{-1} PIPES buffer, pH 7) for 0.13, 1, 30, and 63 d. The experiments were performed in 160 mL serum bottles with butyl rubber stoppers and Al crimp-seals at 30 °C and 25 rpm horizontal shaking. Unlike the AH_2DS experiments, bicarbonate additions were not made to these experiments to avoid siderite precipitation.

2.5. Analyses

After equilibration, the ferrihydrite suspensions were sampled in an anaerobic (N_2:H_2, 95:5) glove bag (Coy Laboratory Products Inc., Grass Lake, MI). Approximately, 0.4 mL of suspension filtrate (0.2 μm; after discarding first 20 drops) was combined with 0.4 mL of 1 mol L^{-1} HCl in an eppendorf tube, for aqueous Fe(II) measurements. Acid-extractable Fe(II) was obtained by placing a 0.4 mL aliquot of the suspension into 0.4 mL of 1 mol L^{-1} HCl or 10 mol L^{-1} HCl and equilibrating for 24 h. The higher acid concentration was used when crystalline phases, goethite and magnetite primarily, were the transformation products. The HCl extracts and aqueous fractions were analyzed for Fe(II) by the ferrozine assay (Stookey, 1970). Fe_{total} and P concentrations were determined on select samples using inductively coupled plasma emission spectroscopy (ICP). Suspension filtrates from the AH_2DS experiments (<0.2 μm) were diluted in anoxic water, sealed in cuvettes, removed from the glove bag, and scanned from 500 to 300 nm with a Shimadzu UV/VIS spectrophotometer to measure the absorbance of AQDS at 325 nm and of AH_2DS at 386 nm (Liu et al., 2007a).

2.5.1. ^{57}Fe-Mössbauer spectroscopy, X-ray diffraction, and electron microscopy

Mössbauer samples were created by filtering (0.45 μm) ~5 mL of the mineral suspension under anoxic conditions. The resulting filter membrane containing the moist mineral residue was placed into a Cu sample holder that was filled with petroleum jelly and sealed at both ends with scotch tape (another sub-sample of the suspension was dried in the anaerobic chamber for XRD and microscopy). An O_2 impermeable polymer (aluminized Mylar) was used as a seal at each end of the holder. Both the tape and polymer were snapped into the holder with rings made of PEEK polymer. The Mössbauer disks were stored in the anoxic chamber until analysis.

Mössbauer spectra were collected using a 50 mCi (initial strength) ^{57}Co/Rh source. The velocity transducer MVT-1000 (WissEL) was operated in a constant acceleration mode (23 Hz, ±12 mm/s). An Ar–Kr proportional counter analyzed transmitted radiation, and the counts were stored in a multichannel scalar (MCS) as a function of energy (transducer velocity) using a 1024 channel analyzer. Data were folded to 512 channels to give a flat background and a zero-velocity position corresponding to the center shift (CS) of a metal iron foil at room temperature (RT). Calibration spectra were obtained with a 25 μm thick α-Fe(m) foil (Amersham, England) placed in the same position as the samples to minimize sample geometry errors. A closed-cycle cryostat (ARS, Allentown, PA) was employed for low temperature measurements. The Mössbauer data

Table 1
Chemical composition of various treatments.

Treatment	Description	Fe(III) in 2-line Si Ferrihydrite $\times 10^{-3}$ mol L^{-1}	$Fe(II)_{aq}$ $\times 10^{-3}$ mol L^{-1}	AH_2DS $\times 10^{-3}$ mol L^{-1}	$Fe(II)_{equiv}$[b] $\times 10^{-3}$ mol L^{-1}	$Fe(II)_{equiv}$/ Fe(III)[c]	NaH_2PO_4 $\times 10^{-3}$ mol L^{-1}	$NaHCO_3$ $\times 10^{-3}$ mol L^{-1}	AH_2DS/ Fe	P/(Fe + P) or (%P)[a]	C/(Fe + C) or (%C)[a]
1	AH_2DS, −P, −C (PIPES)	31.4	–	1.5	3.0	0.11	–	–	0.05	–	–
2	AH_2DS, −P, +C (PIPES)	31.4	–	1.5	3.0	0.11	–	0.25	0.05	–	0.008 (0.8%)
3	AH_2DS, −P, +C (PIPES)	31.4	–	1.5	3.0	0.11	–	0.75	0.05	–	0.024 (2.4%)
4	AH_2DS, +P, −C (PIPES)	31.4	–	1.5	3.0	0.11	0.6	–	0.05	0.02 (2%)	–
5	AH_2DS, +P, +C (PIPES)	31.4	–	1.5	3.0	0.11	0.6	0.75	0.05	0.02 (2%)	0.024 (2.4%)
6	AH_2DS, −P, −C (PIPES)	23.5	–	3.75	7.5	0.54	–	–	0.175	–	–
7	AH_2DS, +P, −C (PIPES)	23.5	–	3.75	7.5	0.54	0.3	–	0.175	0.02 (2%)	–
8	$Fe(II)_{aq}$, −P (PIPES)	10	1.0	–	0.5	0.05	–	–	–	–	–
9	$Fe(II)_{aq}$, +P (PIPES)	10	1.0	–	0.5	0.05	0.2	–	–	0.02 (2%)	–
10	$Fe(II)_{aq}$, −P (PIPES)	10	3.3	–	3.3	0.33	–	–	–	–	–
11	$Fe(II)_{aq}$, +P (PIPES)	10	3.3	–	3.3	0.33	0.2	–	–	0.02 (2%)	–
12	$Fe(II)_{aq}$, −P (PIPES)	10	5.0	–	5	0.50	–	–	–	–	–
13	$Fe(II)_{aq}$, +P (PIPES)	10	5.0	–	5	0.50	0.2	–	–	0.02 (2%)	–

[a] Mole fractions are shown as %P and %C in parentheses.

[b] The concentration of Fe(II) resulting from AH_2DS oxidation or direct Fe(II) addition.

[c] Assumes 100% oxidation for AH_2DS experiments: $Fe(II)_{equiv}/Fe(III) = 2[AH_2DS]/(Fe(III)_{initial} - 2[AH_2DS])$. For $Fe(II)_{aq}$ experiments: $Fe(II)_{equiv} = Fe(II)_{aq}/Fe(III)_{initial}$ where $Fe(III)_{initial} = Fe(III)$ in 2-line Si ferrihydrite. Note that $Fe(II)/Fe(III) = 0.5$ for stoichiometric magnetite. Values of 0.67, 1.0, and 6.7 mmol Fe(II)/g of ferrihydrite reported by Hansel et al. (2005), represent $Fe(II)_{equiv}/Fe(III)$ ratios of 0.083, 0.12, and 0.83, respectively. The value of 1.0 mmol Fe(II)/g of ferrihydrite or $Fe(II)_{equiv}/Fe(III) = 0.124$ is reported by Hansel et al. (2005) as a threshold value for magnetite formation.

were modeled with the *Recoil* software (University of Ottawa, Canada) using a Voigt-based structural fitting routine (Rancourt and Ping, 1991). The coefficient of variation of the spectral areas of the individual sites generally ranged between 1% and 2% of the fitted values.

Powder XRD patterns for mineral residues 1–7 (Table 1) were obtained with a Philips PW3040/00 X'pert MPD system, using CuK_α radiation with a variable divergent slit and a solid-state detector. The routine power was 700 W (35 kV, 20 mA). Mineral suspensions were filtered through a 0.2 μm nylon filter and dried under anoxic conditions. The powder samples were packed into wells (1/4 inch diameter and 1/32 inch deep) of low-background quartz XRD slides. Packing was carried out in the anoxic chamber, but XRD measurements were performed in ambient atmosphere. An earlier study (Kukkadapu et al., 2004) showed little oxidation of the dried powders during XRD analysis.

In order to alleviate concerns over oxidation during XRD analyses, mineral residues from the $Fe(II)_{aq}$ experiments (#8–13, Table 1) were analyzed as a moist paste in sealed micro-capillaries (0.5 mm). The capillaries were filled in an anoxic glovebox ($O_2 < 0.5$ ppm). A Rigaku D/MAX-

Table 2
Mineral products of ferrihydrite reaction with AH_2DS and $Fe(II)_{aq}$.

Treatment	Description	$Fe(II)_{equiv}/Fe(III)$	Final pH	Mineralogy		
				0.13 d	1 d	30 d
1	AH_2DS, −P, −C (PIPES)	0.11	7.3	2LF	2LF	L>>G
2	AH_2DS, −P, +C (PIPES)	0.11	7.0		L>>G	L>>G
3	AH_2DS, −P, +C (PIPES)	0.11	8.0	2LF>>G*	G*	G
4	AH_2DS, +P, −C (PIPES)	0.11	7.4	2LF	2LF/6LF	2LF/6LF
5	AH_2DS, +P, +C (PIPES)	0.11	8.0	2LF	2LF/6LF	2LF/6LF
6	AH_2DS, −P, −C (PIPES)	0.54	7.5	2LF	2LF/M*	M
7	AH_2DS, +P, −C (PIPES)	0.54	7.6	2LF	2LF/M*	M
8	$Fe(II)_{aq}$, −P (PIPES)	0.05	6.8	L	L	L
9	$Fe(II)_{aq}$, +P (PIPES)	0.05	6.8	F>>>L	F>L	L
10	$Fe(II)_{aq}$, −P (PIPES)	0.33	6.7	L	L	L>M
11	$Fe(II)_{aq}$, +P (PIPES)	0.33	6.7	F>>L	F>L	L
12	$Fe(II)_{aq}$, −P (PIPES)	0.50	6.5	L	L	L≈M
13	$Fe(II)_{aq}$, +P (PIPES)	0.50	6.5	F>>L	F>>L	L>>M

2LF, 2 line ferrihydrite[a]; 6LF, 6 line ferrihydrite[a]; F, undifferentiated ferrihydrite; L, lepidocrocite; G, goethite; G*, incipient goethite; M, magnetite; M*, incipient magnetite.
2LF and 6LF not discernable from one-another by capillary XRD used for $Fe(II)_{aq}$ experiments.

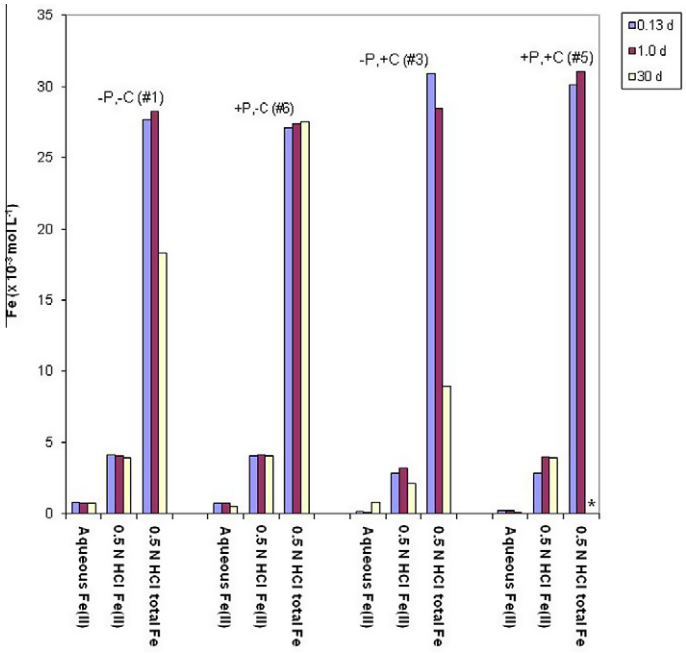

Fig. 1. Aqueous Fe(II), 0.5 N HCl Fe(II), and Fe_{total} of 2-line Si-ferrihydrite reacted with AH_2DS at $Fe(II)_{equiv}/Fe(III) = 0.11$. The experiment numbers in Table 1 are noted. *Total Fe analysis at 30 d not available.

Rapid II microdiffraction system was used in transmission mode. Cu Kα X-rays were generated using a 1200 W rotating anode source and collimated to 100 μm on the capillary surface, with diffraction pattern collection onto a 2-D detector. The capillary tubes and water contribute to the diffraction pattern and must be considered (Figs. EA-1 and EA-2). The JADE+, V5 (Materials Data Inc., Livermore, California) software package was used for data analysis.

Scanning electron microscopy (SEM) was performed on powder samples using a FEI Helios 600 Dual Beam spectrometer operating at 5 keV at 3–4 mm working distance fitted with secondary and backscatter electron detectors. High-resolution TEM analysis was carried out on a Jeol JEM 2010 microscope fitted with a LaB_6 filament and an acceleration voltage of 200 kV. All images were recorded using a 1 × 1 K CCD camera and processed using Digital Micrograph (Gatan, USA). Lattice plane space was measured using the selected area electron diffraction (SAED) method. The camera constant of the microscope was calibrated using an evaporated Al polycrystalline thin film, which yields an overall measurement accuracy within the error of 1.4%.

3. RESULTS

3.1. General observations

The reaction of either AH_2DS or $Fe(II)_{aq}$ with 2-line ferrihydrite in PIPES buffer produced 6-line ferrihydrite, lepidocrocite, goethite, or magnetite as products (Table 2).

Lepidocrocite was most common, especially with $Fe(II)_{aq}$ as the reactant, where it formed rapidly in the absence of P. Goethite was observed with AH_2DS primarily when bicarbonate was present in the media (e.g., #2 and #3). Siderite was not observed when bicarbonate was present under the experimental conditions used. Magnetite was observed with both reductants at the highest $Fe(II)_{equiv}$/Fe(III) ratios (#7, #8, #12). P suppressed reductive recrystallization at all reductant concentrations (#4, #5, #9, #11), and was especially inhibitory to magnetite formation by $Fe(II)_{aq}$ (#13). The final pH of the experiments varied by 1.5 U (Table 2) with the lowest values observed for experiments with $Fe(II)_{aq}$. Details follow where results are presented in terms of the $Fe(II)_{equiv}$/Fe(III) ratio (Table 1).

3.2. AH_2DS reacted with 2-line Si-ferrihydrite

3.2.1. Ferrihydrite transformation with $Fe(II)_{equiv}$/Fe(III) = 0.11

AH_2DS reacted (oxidized) to completion with ferrihydrite within 0.13 d as confirmed by UV–VIS absorption spectroscopy (not shown). In all four treatments, 10–15% of the initially added Fe(III) was reduced within this time period (e.g., 0.5 mol L^{-1} HCl Fe(II); Fig. 1). The oxidation of AH_2DS to AQDS is a two-electron transfer reaction that is coupled, in this case, to the heterogeneous reduction of ferrihydrite Fe(III) to Fe(II) (Burgos et al., 2003). Aqueous Fe(II) constituted 10–20% of the 0.5 mol L^{-1} HCl Fe(II) [e.g., $Fe(II)_{total}$]. Sorbed Fe(II), calculated as the difference between 0.5 mol L^{-1} HCl Fe(II) and aqueous Fe(II), was ~10% of the total solid Fe. The pretreatment of 2-line ferrihydrite with P(2%) and/or C(2.4%) had little effect on the extent or timing of 2-line ferrihydrite reduction (Fig. 1). Total 0.5 mol L^{-1} HCl extractable Fe decreased at 30 d in those samples where appreciable crystalline Fe(III) oxide formation was observed [−P−C(#1); −P+C(#3)]. For the others (e.g., +P treatments), Fe(II) concentrations (aqueous and 0.5 mol L^{-1} HCl-extracted) and 0.5 mol L^{-1} HCl total Fe were similar at all the time points. Crystalline Fe(III) oxides, such as goethite and lepidocrocite, are less soluble in weak acid than ferrihydrite (Fredrickson et al., 1998).

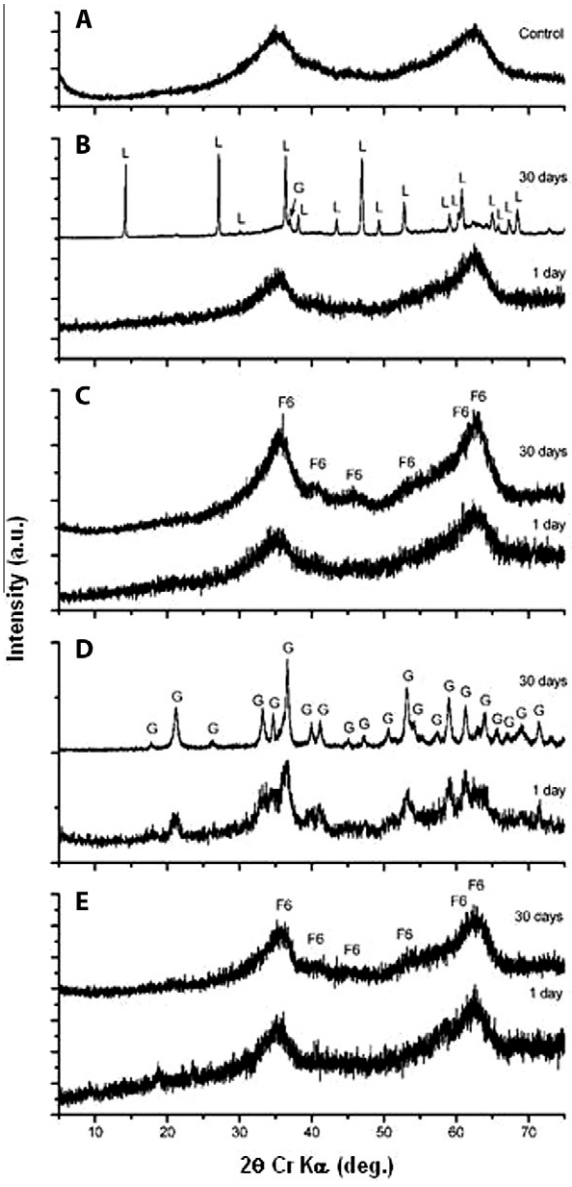

Fig. 2. Reaction products from the $Fe(II)_{equiv}$/Fe(III) = 0.11 experiment series (A) Control; (B) −P−C (#1); (C) +P−C (#4); (D) −P+C (#3); and (E) +P+C (#5). Lepidocrocite (L), goethite (G), and 6-line ferrihydrite (F6) are labeled.

In spite of similar reduction extents and aqueous and sorbed Fe(II) concentrations, the mineralogic nature of the reductive transformation products varied with pretreatment. Without P or C (#1), 2-line ferrihydrite slowly transformed to lepidocrocite (Fig. 2B). The slow nature of the transformation reaction was evident from a comparison of the 1 and 30 d XRD patterns (Fig. 2B). The 1 d pattern was virtually identical to that of the control (Fig. 2A), in

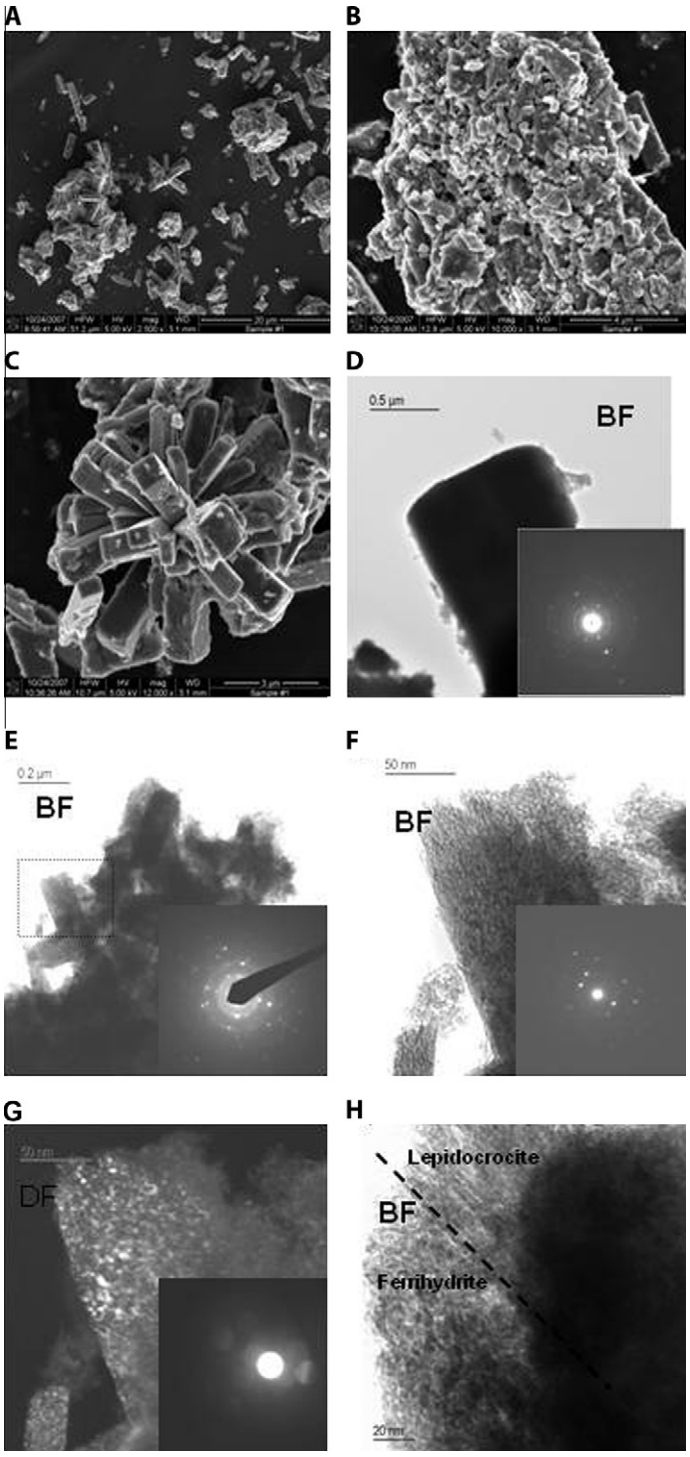

Fig. 3. SEM (A–C) and transmission electron micrographs (D–H) of 2-line Si-ferrihydrite reacted with AH_2DS [$Fe(II)_{equiv}/Fe(III)$] = 0.11 without P or C (30 d). The product consisted of lepidocrocite laths (A), plates (B), and rosettes (C) intermixed with 2-line Si-ferrihydrite. The TEM–SAED (D–F inserts) and nanodiffraction (insert G) of the product phases were consistent with compact lepidocrocite (PDF #044-1415) crystals relatively free of ferrihydrite association (D), and porous lepidocrocite crystals with ferrihydrite interface (E–H). The bright field (BF) and dark field (DF) images shown in (F) and (G) correspond to the region highlighted in (E).

spite of significant sorbed Fe(II) (e.g., 10%; Fig. 1). The +P (#6) was partially transformed to Fe(II)-sorbed, 6-line ferrihydrite over 30 d (Fig. 2C), with no hints of lepidocrocite or goethite. Ferrihydrite pretreatment with C facilitated transformation to crystalline Fe(III)-oxides (Table 2 and Fig. 2D). The product identity was dictated by the C concentration. Lepidocrocite formed in the low + C treatment (0.8%; #2, not shown), whereas goethite precipitated when C was present at 2.4% (#3, Fig. 2D). The effect of C was, however, suppressed by 2% P (#5, Fig. 2E), yielding 6-line ferrihydrite as the product.

SEM analysis (Fig. 3) of the lepidocrocite/ferrihydrite mixture obtained after 30 d without P or C (#1, Fig. 2B) revealed the presence of lepidocrocite in various morphologies intermixed with 2-line ferrihydrite. Lepidocrocite existed in 2–5 μm lath-like and tabular morphologies. The crystallites were both isolated (Fig. 3A and B) and present as rosettes (Fig. 3A–C). Dark field (DF) and bright field (BF) TEM imaging as well as SAED and nanodiffraction analyses revealed two distinct lepidocrocite crystal formations: (i) compact (Fig. 3D) and (ii) porous (Fig. 3E–G). High-resolution TEM imaging of the porous lepidocrocite/ferrihydrite region further revealed an apparent interface between lepidocrocite and ferrihydrite (Fig. 3H).

The nature of 2- and 6-line ferrihydrite and their spatial association in the +P−C system (#4, Fig. 2C) was further investigated using BF and DF TEM and associated SAED measurements (Fig. 4). Bright spots in the DF images were attributed to more crystalline 6-line ferrihydrite that was randomly dispersed through the 2-line ferrihydrite. The 2- to 6-line ferrihydrite ratio estimated by TEM was 30:70, which was in qualitative agreement with the XRD pattern (Fig. 2C).

SEM and TEM analysis (Fig. 5) of the goethite/ferrihydrite mixture from the −P+C (2.4%) treatment (#3, Fig. 2D) revealed the presence of acicular goethite (20–200 nm) with individual and intergrown crystallites (Fig. 5A and B), that were intimately associated with ferrihydrite (Fig. 5C–E). It is unclear whether the observed goethite–ferrihydrite association is characteristic of the mineral product, or an artifact of sample preparation that included drying.

Mössbauer spectroscopy measurements were performed to characterize the sorbed Fe(II) that resulted from heterogeneous reaction with AH_2DS. The Fe(II)-containing 2- and 6-line ferrihydrite mixture that was free of goethite or lepidocrocite [+P−C; #4; Fig. 2C] and another containing lepidocrocite, goethite, and ferrihydrite [−P+C(2.4%); #3; Fig. 2D) were analyzed. The derived Mössbauer parameters of the control Si-ferrihydrite [center shift, {CS = 0.46 mm/s}, sensitive to oxidation state; and average quadrupole splitting, {QS = 0.83 mm/s}, sensitive to coordination environment] at RT (not shown) and 77 K (Fig. 6A) agreed well with that of 2-line ferrihydrite (Murad and Cashion, 2004).

The RT spectrum of the Fe(II)-ferrihydrite (+P−C; #4) displayed a large central doublet due to residual ferrihydrite

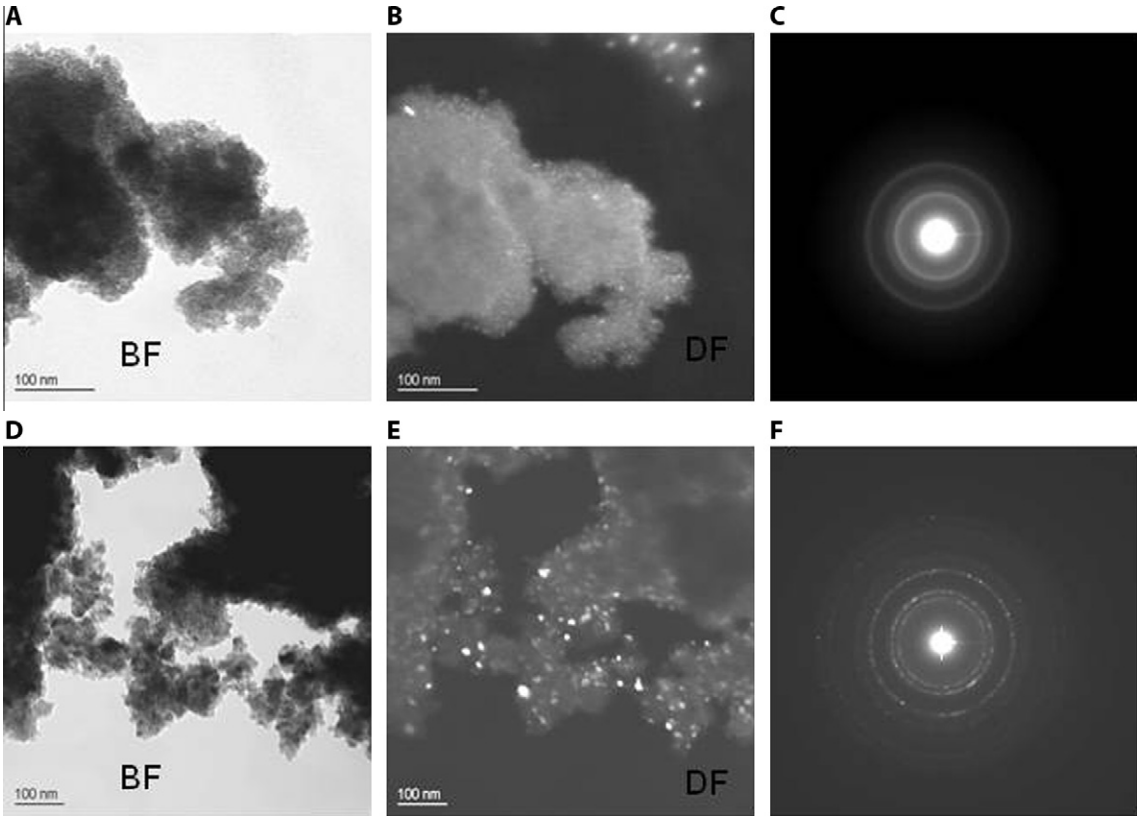

Fig. 4. TEM and TEM–SAED of 2-line Si-ferrihydrite reacted for 30 days with AH_2DS (+P−C) displaying partial transformation of 2-line ferrihydrite to 6-line ferrihydrite. The bright spots in dark field (DF) images result from 6-line ferrihydrite (B and E). The ring pattern in (C) was characteristic of 2-line ferrihydrite, while that in (F) was due to 6-line ferrihydrite.

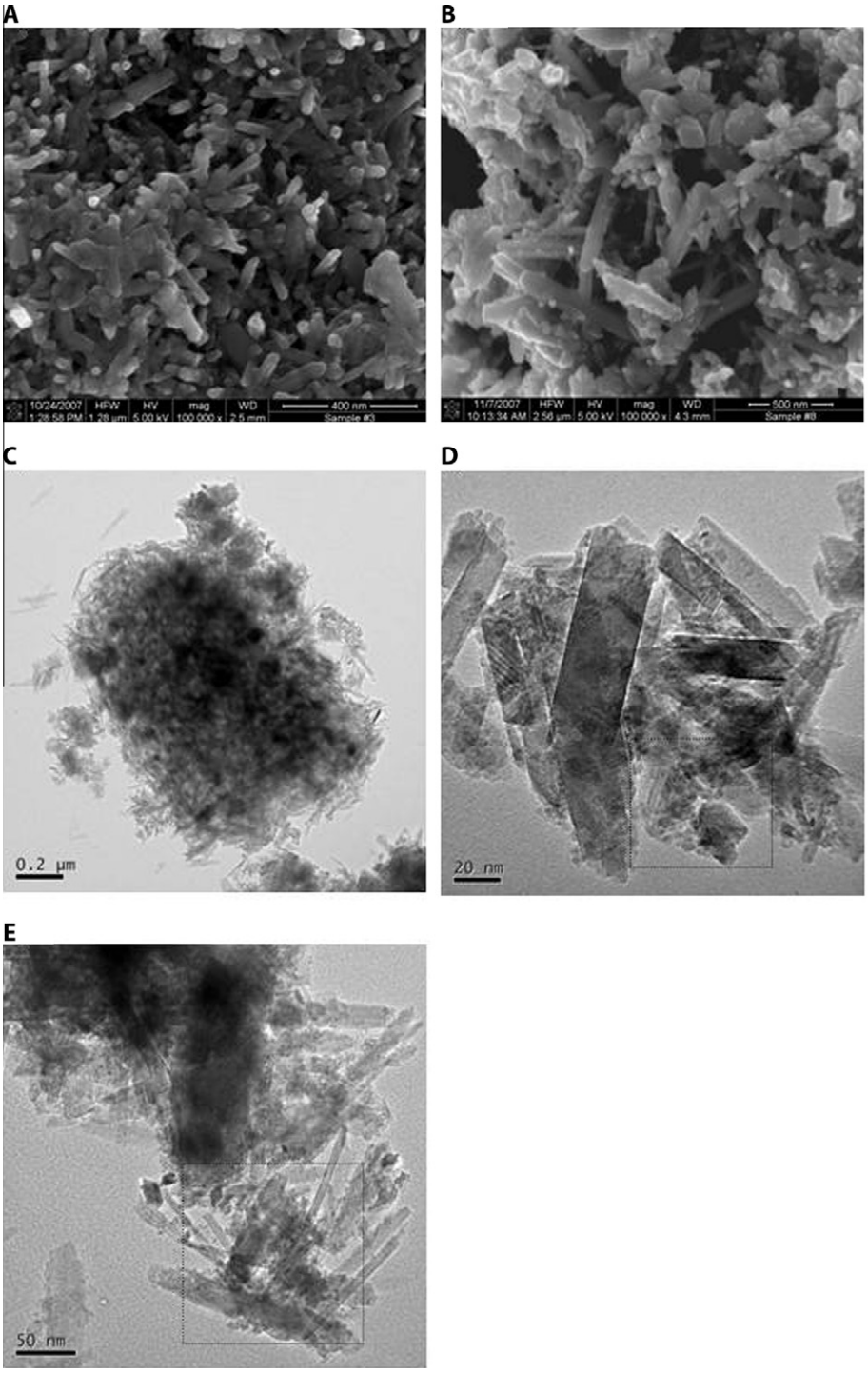

Fig. 5. SEM (A and B) and TEM bright field (C–E) of 2-line Si-ferrihydrite reacted for 30 days with AH_2DS in presence of C (2.4%). The highlighted regions in TEM (D and E) revealed association of acicular goethite crystals with ferrihydrite.

(~90% of spectral area), and a small, broad doublet from sorbed Fe(II) (~10%; indicated by * in Fig. 6B). The 77 K spectrum, on the other hand, displayed a distinct Fe(II) doublet, a Fe(III) doublet, and a Fe(III) sextet (Fig. 6C). The spectral differentiation of Fe(III) at 77 K was consistent with the presence of both 2- and 6-line ferrihydrite (Kukkadapu et al., 2003). The contribution of the Fe(III)-sextet to the spectrum (~35%), however, was lower than the estimated 6-line ferrihydrite concentration from XRD and TEM (~70%). This discrepancy may result from decreased inter-particle magnetic interactions or hyperfine fields due to P surface complexation as reported for Si-doped ferrihydrites (Zhao et al., 1996). The explicit contributions of the 2- and 6-line components to the spectra were consequently not modeled because of these uncertainties.

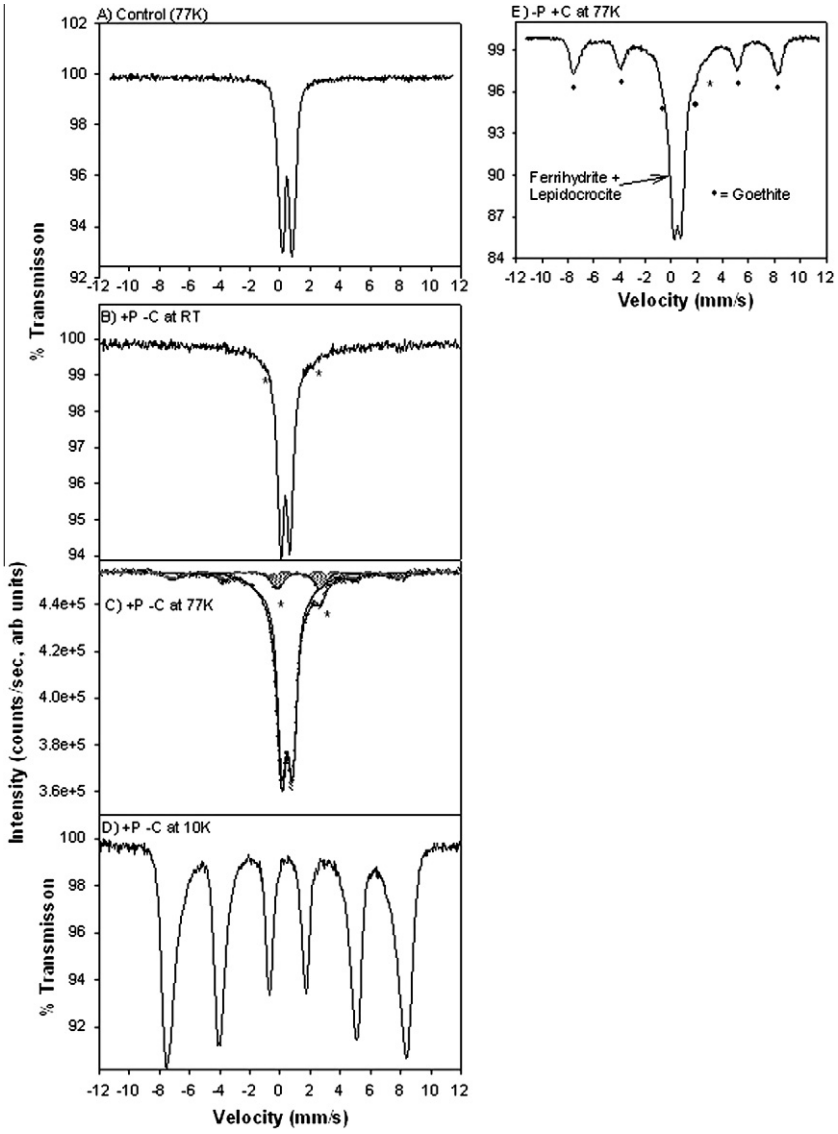

Fig. 6. Mössbauer spectra of control at 77 K (A), and spectra of 2-line Si-ferrihydrite reacted for 30 days with AH_2DS and +P−C (#4) at various temperatures (B–D) or −P+C (#3) (E). Fe(II) doublet peaks are indicated by * in (B), (C), and (E). The Fe(II) doublet peaks in (C) are also textured with dots.

The ferrous doublet contribution to the +P−C spectra (Fig. 6B and C) was consistent with the 0.5 mol L^{-1} HCl extractable Fe(II) concentration (~10%). The Fe(II) spectral area was higher than the maximum amount of vivianite (3%) that could form, given the P/(Fe + P) ratio of 2% used in the experiment (Table 1). The derived Fe(II) Mössbauer parameters were also different from those of vivianite (e.g., Kukkadapu et al., 2004; Murad and Cashion 2004). The Fe(II) and ferrihydrite phases magnetically ordered at 10 K (Fig. 6D). The RT and 77 K Mössbauer parameters [asymmetric QS distribution and |QS|] and the 10 K temperature behavior implied that the sorbed Fe(II) was: (i) distributed over a range of sites (Rancourt and Ping, 1991), (ii) in distorted octahedral coordination (Greenwood and Gibb, 1971), and (iii) strongly bound as an inner-sphere complex to Fe(III)-O sites (Greenwood and Gibb, 1971). Discrete Mössbauer peaks characteristic of Fe(II) were also evident in the spectra of the lepidocrocite/goethite/ferrihydrite mixture (−P+C; #3, Fig. 6E). Quantification and interpretation of the Fe(II) signal for this treatment was complicated by low signal strength and peak overlap with the ferric doublet and sextet.

3.2.2. Ferrihydrite transformation with $Fe(II)_{equiv}$/Fe(III) = 0.54

The $Fe(II)_{equiv}$/Fe(III) ratio of this experiment was approximately equal to that of magnetite after the heterogeneous reaction with AH_2DS was complete (e.g., 1:2). Approximately 33% of the total Fe was reduced in 1 d for both experiments (#6 and #7), consistent with complete AH_2DS oxidation (Fig. 7A). Stronger acid (5 mol L^{-1} HCl) was used to dissolve the crystalline products that formed under these conditions. Both the −P and +P experiments displayed almost identical aqueous and extractable

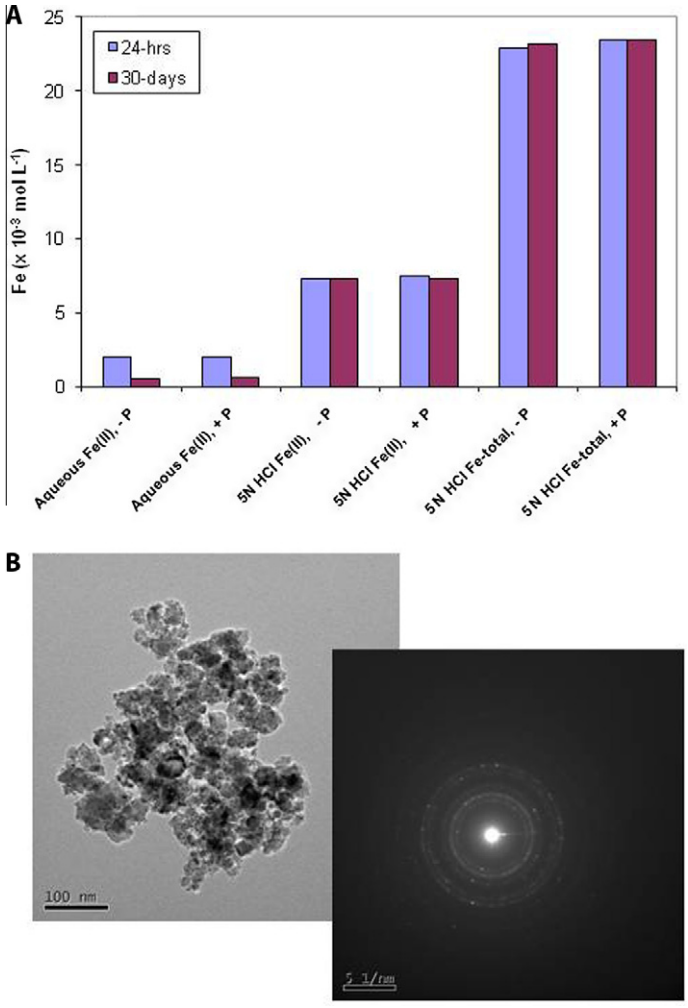

Fig. 7. Iron concentrations (A) after 1 and 30 d of AH_2DS reaction with ferrihydrite at $Fe(II)_{equiv}/Fe(III) = 0.5$. Product morphology (30 d) and selected area diffraction (SAED) by TEM (B).

Fe. Aqueous Fe(II) represented 23% of the Fe(II) pool after 1 d, and this decreased by a factor of 2.5 over 30 d. Little change in extractable Fe was noted between 1 and 30 d.

Incipient magnetite was observed in both experiments after 1 d, and this crystallized to magnetite in 30 d (Fig. 8). Phosphate had no apparent effect on the 30 d product of reaction. The final product was stoichiometric magnetite in both treatments (#6 and #7) as determined by both chemical extraction [e.g., 30% Fe(II) in Fig. 7A] and Mössbauer analysis (not shown). There was no evident crystalline precursor. The magnetite existed as irregular 20–45 nm crystallites without distinct morphology as determined by TEM/SAED (Fig. 7B). A solid-state transformation reaction was implied.

3.3. $Fe(II)_{aq}$ reacted with 2-line Si-ferrihydrite

3.3.1. Aqueous Fe(II) concentrations

The Fe(II) experiments were performed with 10×10^{-3} mol L^{-1} ferrihydrite and involved contact with 0.5, 3.3, and 5.0×10^{-3} mol L^{-1} $Fe(II)_{aq}$ both with and without P (Table 1). All of these experiments supported significant $Fe(II)_{aq}$ concentrations during their course (Fig. 9). While there were temporal changes in $Fe(II)_{aq}$ that varied with treatment, there were no consistent trends, and the degree of variation was small. Ferrous iron adsorption, and hence electron transfer to ferrihydrite, was rapid and effectively complete by the first measurement point (0.13 d). The degree of Fe(II) adsorption was approximately 55% for 0.5×10^{-3} mol L^{-1}, and 15% for 3.3 and 5.0×10^{-3} mol L^{-1} Fe(II). Consequently, most of the added $Fe(II)_{aq}$ remained in solution for the two highest concentrations.

3.3.2. Ferrihydrite transformations

The reductive transformation of Si-ferrihydrite was consistent across the Fe(II) concentration range studied (Figs. 10, 11 and EA-3). Quantification of residual ferrihydrite in these samples by XRD was more difficult than the powders because of water and capillary interferences (Figs. EA-1 and EA-2). Changes to the intensity of the XRD peaks of all samples were minimal between 30 and 63 d (Figs. EA-3–EA-5), indicating complete transformation of ferrihydrite by 30 d. Moreover, there was no change in the product

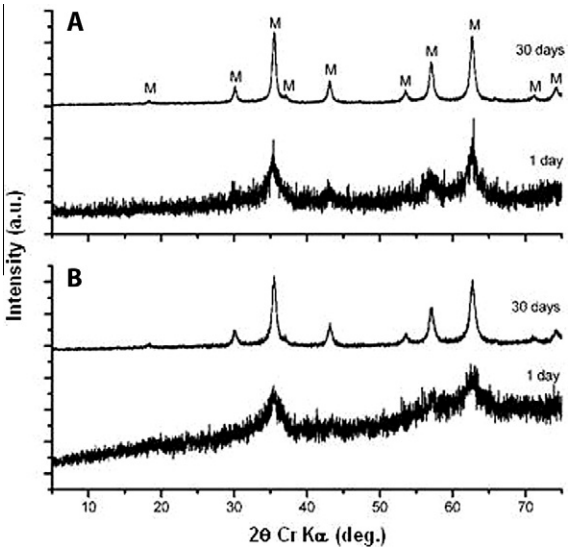

Fig. 8. Powder X-ray diffraction of dried mineral residues after 1 and 30 d of AH_2DS reaction with ferrihydrite at $Fe(II)_{equiv}/Fe(III) = 0.54$. (A) −P−C (#6) and (B) +P−C (#7). Magnetite (M) peaks are labeled.

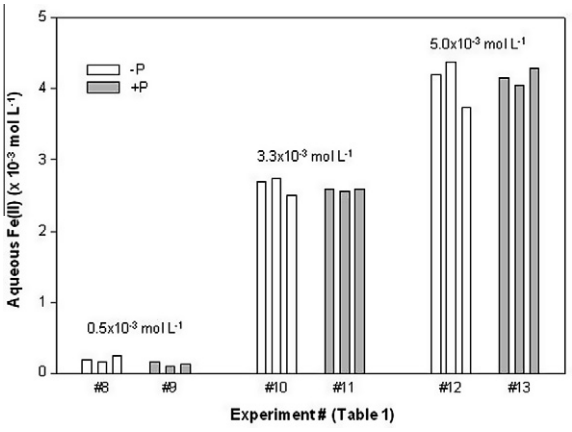

Fig. 9. Aqueous Fe(II) concentrations present in treatments #8–13 as measured after 0.13, 1.0, and 30 d of contact. The ferrihydrite concentration was 10×10^{-3} mol L^{-1} and the initial $Fe(II)_{aq}$ concentrations were as noted.

phase assemblages between 30 and 63 d, indicating reaction product stability over this time range.

Lepidocrocite formed rapidly in the absence of P, with approximately 35% of the ferrihydrite transformed within 0.13 d for all three Fe(II) concentrations. At 0.5×10^{-3} mol L^{-1} $Fe(II)_{aq}$, lepidocrocite formation increased by 1.5 times between 0.13 and 1 d, and another 2 times between 1 and 30 d (Fig. 10). Product lepidocrocite exhibited tabular morphology (~1 μm) with predominant {0 1 0} faces (Fig. 12), as described by Schwertmann and Cornell (2000). The lath-like rosettes and porous structures observed with AH_2DS (Fig. 3) were not evident here. At 5.0×10^{-3} mol L^{-1}, lepidocrocite formation was static between 0.13 and 1 d, but increased by 1.5 times over 30 d.

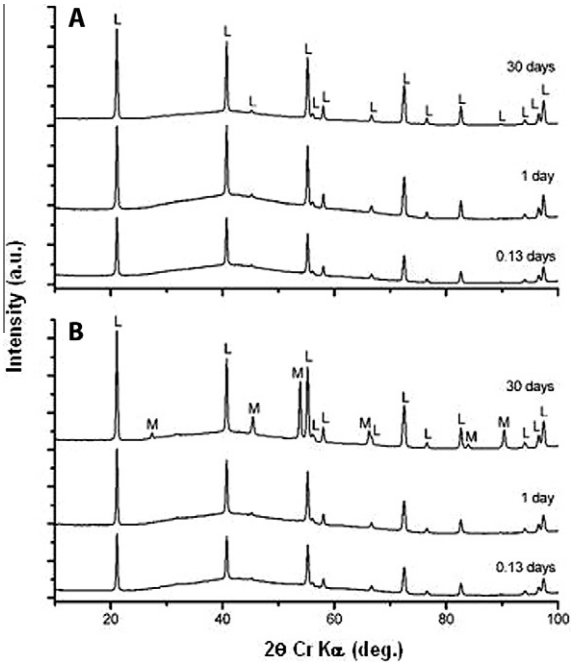

Fig. 10. Capillary X-ray diffractograms of moist mineral residue from the reaction of 0.5×10^{-3} mol L^{-1} $Fe(II)_{aq}$ (A) or 5.0×10^{-3} mol L^{-1} $Fe(II)_{aq}$ (B) with 10×10^{-3} mol L^{-1} Si-ferrihydrite. Diffraction peaks from lepidocrocite (L) and magnetite (M) are labeled.

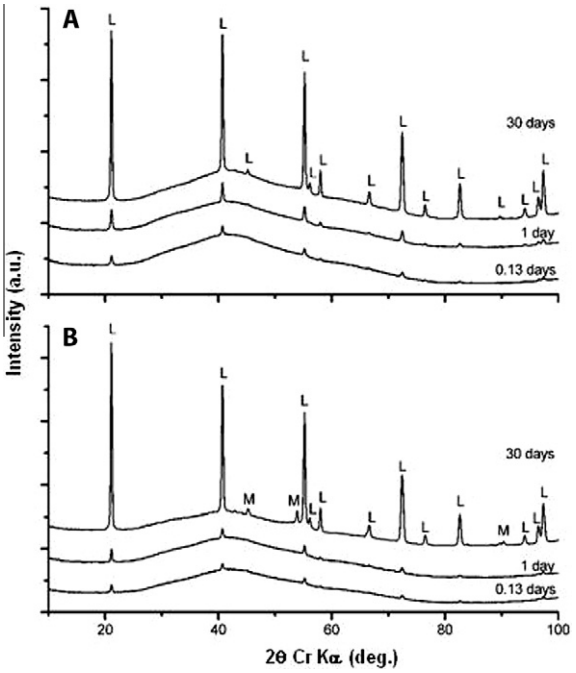

Fig. 11. Capillary X-ray diffractograms of moist mineral residue from the reaction of 0.5×10^{-3} mol L^{-1} $Fe(II)_{aq} + 0.2 \times 10^{-3}$ mol L^{-1} $PO_{4(aq)}$ (A), or 5.0×10^{-3} mol L^{-1} $Fe(II) + 0.2 \times 10^{-3}$ mol L^{-1} $PO_{4(aq)}$ (B) with 10×10^{-3} mol L^{-1} Si-ferrihydrite. Diffraction peaks from lepidocrocite (L) and magnetite (M) are labeled.

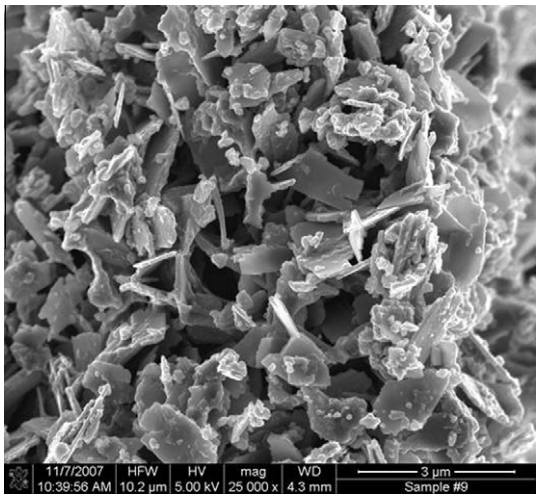

Fig. 12. SEM micrograph of tabular lepidocrocite produced from the reaction of $Fe(II)_{aq}$ with Si-ferrihydrite.

Magnetite formation commenced after 1 d at 5.0×10^{-3} mol L^{-1} Fe(II), and continued in parallel to, but with a faster rate than lepidocrocite to 30 d (Fig. 10). The mineralization trend for 3.3×10^{-3} mol L^{-1} Fe(II) was nearly identical to 5.0×10^{-3} mol L^{-1}, except that lesser amounts of magnetite were formed after 30 d (Fig. EA-6).

Phosphate had a comparable effect on ferrihydrite transformation at all $Fe(II)_{aq}$ concentrations (Fig. 11 and EA-6). The formation of lepidocrocite was dramatically slowed by P over the first day of reaction. After this inhibition period, lepidocrocite formation proceeded to yield final concentrations after 30 d that were comparable to the system without P. Magnetite formation was also inhibited by P. Magnetite existed only as a minor component after 30 d at 5.0×10^{-3} mol L^{-1}, and was not observed at 3.3×10^{-3} mol L^{-1} (Fig. EA-6). Indeed, the 30 d diffraction pattern for 0.5 and 3.3×10^{-3} mol L^{-1} Fe(II) in the presence of P were virtually identical.

4. DISCUSSION

The research utilized a 2-line ferrihydrite preparation containing 2 mol% Si (0.02 mol Si:mole Fe). Ferrihydrites with comparable Si concentrations are observed in terrestrial environments (Fortin et al., 1993; Tessier et al., 1996; Perret et al., 2000), with sorbed Si promoting their metastable persistence (Carlson and Schwertmann, 1981). Sorbed Si retards ferrihydrite recrystallization under oxic laboratory conditions (Anderson and Benjamin, 1985; Cornell et al., 1987; Cornell and Giovanoli, 1987), and yields ferrihydrite preparations free of crystalline impurities (Dyer et al., 2010). It was used here specifically to eliminate a parallel mineral transformation pathway of oxidative recrystallization. The total sorbed Si concentration (0.02 mol Si:mole Fe) is well below site saturation, according to Dzombak and Morel (1990) (e.g., Type 2 sites at 0.2 mol:mol Fe). ATR-IR measurements of adsorbed silica on ferrihydrite at this surface loading indicate the presence of approximately 75% monomeric surface complexes (Swedlund et al., 2009). Increased surface loadings beyond this value encourage surface polymerization, decreasing concentrations of the monomeric surface complex, and Si precipitation around aggregate surfaces (Swedlund et al., 2009; Dyer et al., 2010). While retarding oxidative recrystallization, we have observed no influence of sorbed Si at this concentration on reductive ferrihydrite mineralization in previous studies (Kukkadapu et al., 2004). We cannot, however, totally discount an effect. Unpublished studies by our laboratory reveal only slight differences in the fundamental reaction rate of AH_2DS with fresh 2-line ferrihydrite precipitate and an identical preparation with 0.02 mol Si:mole Fe. In contrast, significantly higher concentrations of coprecipitated Si (e.g., 0.68 mol Si:mole Fe) change the reductive mineralization behavior of ferrihydrite and suppresses its reactivity with $Fe(II)_{aq}$ (Jones et al., 2009).

4.1. Comparison of reaction products from AH_2DS and $Fe(II)_{aq}$ without P

Bioreduced AQDS (AH_2DS) caused mineralogic transformations of 2-line Si-ferrihydrite through heterogeneous electron transfer that may be approximated as follows:

$$2Fe(OH)_3 + AH2DS + 4H^+ = 2Fe^{2+} + AQDS + 6H_2O$$

The oxidation of AH_2DS coupled to Fe(III) reduction leads to a significant increase in interfacial pH, while subsequent reactions of Fe(II) including surface complexation, surface hydrolysis, and precipitation act to lower pH.

The electron transfer reaction between AH_2DS and 2-line Si-ferrihydrite was rapid, generally reaching completion, e.g., full AH_2DS oxidation, within 3–24 h (Figs. 1 and 7). Product Fe(II), redistributed over that time period to yield both aqueous and sorbed Fe(II), with aqueous Fe(II) decreasing somewhat with aging between 1 and 30 d for $Fe(II)_{equiv}/Fe(III) = 0.54$ only (Fig. 7). There were no significant differences in $Fe(II)_{aq}/Fe(II)_{sorb}$ distributions between the AQDS and $Fe(II)_{aq}$ systems at comparable concentrations. Neither AH_2DS nor its oxidized form displays any measureable distribution to the solid phase (Liu et al., 2007a).

The primary mineral products of AH_2DS reaction (30 d) were lepidocrocite and goethite (when C was present) at low reductant concentrations [$Fe(II)_{equiv}/Fe(III) = 0.11$]), and magnetite at higher concentration [$Fe(II)_{equiv}/Fe(III) = 0.54$]). This product suite was the same observed by Hansel et al. (2005) and Liu et al. (2007b) using $Fe(II)_{aq}$ as the reactant. The presence of bicarbonate encouraged goethite formation over lepidocrocite with AH_2DS as the reactant, as observed by others for the Fe(II) system (Schwertmann and Thalmann, 1976; Cornell and Schwertmann, 2003; Hansel et al., 2005). XRD measurements after the initial 1 d of reaction displayed nascent patterns consistent with the final products when they consisted of goethite (Fig. 2D) and magnetite (Fig. 8). The 1 d XRD pattern of treatment #1 (−P−C) that yielded lepidocrocite (Fig. 2B), however, showed little difference from the control.

Interfacial electron transfer was proposed to be the initial step in the transformation of 2-line ferrihydrite to

lepidocrocite or goethite via dissolution-reprecipitation in suspensions containing $Fe(II)_{aq}$ concentrations comparable to our $Fe(II)_{equiv}/Fe(III) = 0.11$ AH_2DS system (Hansel et al., 2005; Pedersen et al., 2005). The noted presence of various morphologies of lepidocrocite (tabs, elongated cubes or tubes, and rosettes) with both compact and porous crystal structures in our AH_2DS experiments (Fig. 3), implied multiple formation pathways and additional complexity. Tabular lepidocrocite, formed by reductive dissolution and reprecipitation (Cornell et al., 1989a; Cornell and Schwertmann, 2003), is the most commonly reported morphologic form. The tabular morphology was observed in both AH_2DS (Fig. 3B) and $Fe(II)_{aq}$ (Fig. 12) systems. The cube-like/tubular lepidocrocite morphology (Fig. 3A–C) and porous crystal forms (Fig. 3F and G) were distinct to the AH_2DS system, and implied a second mechanism of growth. The buried interface (Fig. 3H) indicated growth of lepidocrocite from ferrihydrite by aggregation, as noted previously for a biotic system with co-associated goethite and ferrihydrite (Banfield et al., 2000). Selected area diffraction (SAED) and nanodiffraction (Fig. 3F and G) revealed that the crystallographic axes of all the particles in the aggregate were parallel, with the same three-dimensional orientation. The SAED patterns of this material matched well with lepidocrocite, while the aggregate behaved as a single crystal under nanodiffraction (Fig. 3F and G). The compact crystals (Fig. 3D) also displayed lepidocrocite SAED patterns, but their formation pathways, e.g., dissolution–reprecipitation or porous crystal maturation were not discernable.

Small amounts of C in PIPES buffer (>0.8%) facilitated the transformation of 2-line Si-ferrihydrite by AH_2DS to goethite (Fig. 2D) instead of lepidocrocite. Others (Cornell et al., 1989b; Carlson and Schwertmann, 1990) have observed that ferrihydrite transformation to lepidocrocite and/or goethite by $Fe(II)_{aq}$ and L-cysteine is influenced by C concentration. L-Cysteine/cystine has a similar half-cell potential to AQDS (Jones et al., 2004), but is adsorbed more strongly by ferrihydrite. Bicarbonate is believed to suppress lepidocrocite nucleation (Cornell et al., 1989a). Acicular goethite crystals with proximate ferrihydrite were common in this study (Fig. 5D and E), indicating direct transformation from ferrihydrite with time (Hansel et al., 2005). A goethite precursor, such as 6-line ferrihydrite, was not evident by XRD (Fig. 2D). There was no evidence for aggregation-induced crystallization of goethite in presence of C, and goethite was not observed as a precursor to magnetite formation as reported by Coker et al. (2008).

Five differences were observed in ferrihydrite transformation by AH_2DS as compared to $Fe(II)_{aq}$ in the absence of P: (i) the formation rate of lepidocrocite was more rapid in presence of $Fe(II)_{aq}$ at all $Fe(II)_{equiv}/Fe(III)$ ratios, (ii) multiple morphologic forms of lepidocrocite were observed with AH_2DS as the reactant, while $Fe(II)_{aq}$ produced only tabular forms, (iii) AH_2DS was more effective then $Fe(II)_{aq}$ in promoting magnetite formation at higher $Fe(II)_{equiv}/Fe(III)$ ratios, (iv) magnetite formation with $Fe(II)_{aq}$ appeared to occur in parallel with lepidocrocite formation, albeit at slower initial rate, and (v) magnetite formation with AH_2DS appeared to occur by solid-state conversion of aggregated ferrihydrite without a competitive reaction or precursor. We note the possibility that differences between the AH_2DS and $Fe(II)_{aq}$ systems at $Fe(II)_{equiv}/Fe(III) \approx 0.5$ where magnetite formation occurred may have resulted from pH which was one unit higher in the AH_2DS experiment (Table 2). Increasing pH above neutrality promotes magnetite formation (Mann et al., 1989; Faivre et al., 2004; Hansel et al., 2005).

Differences were also observed between our $Fe(II)_{aq}$ system results and those of Hansel et al. (2005), and their resulting conceptual model of $Fe(II)_{aq}$-induced mineralization. Before making these comparisons we note that different starting materials were used. Hansel et al. (2005) used ferrihydrite that was air-dried to form a coating on silica sand, while the experiments described herein utilized a moderately aggregated, Si-substituted, 2-line ferrihydrite suspension. Undoubtedly, differences exist in the fundamental recrystallization rates of these two ferrihydrite preparations as a result of synthesis procedure and history, chemical bonding to the surface of silica (Xu and Axe, 2005), hydration, aggregation, and other physicochemical effects as noted by Kukkadapu et al. (2003). Bearing in mind these differences, there are several significant comparisons. First, Hansel et al. noted that the rates of lepidocrocite precipitation were nearly 10 times faster at higher $Fe(II)_{aq}$. Based on XRD peak height comparisons (Figs. 10, 11 and EA-6), we observed no apparent dependency of lepidocrocite formation on $Fe(II)_{aq}$ concentrations. Second, Hansel et al. noted that magnetite accumulates at the expense of lepidocrocite, implying that lepidocrocite was a precursor to magnetite formation. We observed that magnetite accumulates in parallel with lepidocrocite, albeit at an initially slower rate. Finally, Hansel et al. suggested that the dissolution of lepidocrocite can provide Fe(III) for continued magnetite growth after ferrihydrite has been exhausted. In contrast, we observed that lepidocrocite, once formed, was stable in our experiments for 63 d regardless of $Fe(II)_{aq}$ concentration.

The transformation pathway with 0.5×10^{-3} mol L^{-1} $Fe(II)_{aq}$ and 1.0×10^{-2} mol L^{-1} ferrihydrite was similar to that with AH_2DS at $Fe(II)_{equiv}/Fe(III) = 0.11$, except that the $Fe(II)_{aq}$ system evolved to lepidocrocite much more rapidly (Table 2). Lepidocrocite was also the primary short-term product at higher $Fe(II)_{aq}$ concentrations (3.3×10^{-3} and 5.0×10^{-3} mol L^{-1}) with significant co-existing ferrihydrite (Fig. 10). There was no evidence for green rust in any of our experiments, an often observed precursor of lepidocrocite during Fe(II) oxidation (Cornell and Schwertmann, 2003, and references therein). While Si is recognized to effect the formation of ferrihydrite and its transformation to FeOOH forms under oxidizing conditions (Schwertmann et al., 2004); the level of adsorbed silica in our system had no apparent effect on the rapid formation of lepidocrocite under reducing conditions. Lepidocrocite was the reaction product of ferrihydrite and $FeCl_2$ at $<1 \times 10^{-3}$ mol L^{-1} $Fe(II)_{aq}$ (Hansel et al., 2005; Pedersen et al., 2005; Borch et al., 2007), and the sole short term product at higher concentrations (e.g., 2.0×10^{-3} mol L^{-1} $Fe(II)Cl_2$; Hansel et al., 2005). These past studies suggest that ferrihydrites treated with $>1.0 \times 10^{-3}$ mol L^{-1} Fe(II)

recrystallize to magnetite via "metastable" lepidocrocite. This pathway, however, was not observed in our 3.3×10^{-3} and 5×10^{-3} mol L^{-1} Fe(II) systems, where magnetite formed in parallel to, and not from lepidocrocite (Fig. 10). Beyond this, lepidocrocite showed little metastability as it persisted for 63 d in presence of high $Fe(II)_{aq}$ under conditions that were well within the aqueous stability field of magnetite as revealed by thermodynamic calculation.

4.2. Influence of P

In the $Fe(II)_{equiv}/Fe(III) = 0.11$ AH_2DS system, P(2%) "stabilized" the 2-line Si-ferrihydrite structure from transforming to lepidocrocite (−C, PIPES) or goethite (+C, PIPES). Similar results at comparable P concentrations have been previously reported (Galvez et al., 1999; Borch et al., 2007). Phosphate is strongly adsorbed by ferrihydrite, apparently forming a stable bidentate surface complex at circumneutral pH (Arai and Sparks, 2001; Khare et al., 2007). Strong P adsorption decreases the ferrihydrite transformation rate by preventing the relatively soluble structure from dissolution and subsequent reprecipitation (Biber et al., 1994; Galvez et al., 1999; Majzlan, 2008). Phosphate apparently overwhelms the influence of sorbed (adsorbed or coprecipitated) silica in our ferrihydrite preparation, possibly through competitive displacement, because of its stronger surface complexation (approximately 1000 times greater, Dzombak and Morel, 1990). Previous studies have shown that P displaces co-precipitated Si from ferrihydrite and that the Si concentration used here does not influence reductive ferrihydrite mineralization (Kukkadapu et al., 2004). Sorbed Si is however, important for ferrihydrite stabilization in oxic environments (Carlson and Schwertmann, 1981).

The absence of crystalline Fe(III)-oxides in +P(2%) systems was curious given that $Fe(II)_{aq}$ concentrations and $Fe(II)_{aq}/Fe(II)_{sorb}$ ratios were similar in both the +P and −P systems (Fig. 1). Moreover, the chemical environment of sorbed Fe(II) in samples with and without P was similar as measured by Mössbauer spectroscopy (see * positions in Fig. 6B and E). Mossbauer parameters for the Fe(II) doublet were comparable to sorbed Fe(II) on ferrihydrite as reported by Tronc et al. (1992), and Fe(II) sorbed on hematite above site saturation (Larese-Casanova and Scherer, 2007). This Fe(II) species, however, was different from that identified as: (i) a precursor of green rust in a AQDS- and P-containing MRB system (Kukkadapu et al., 2004), and (ii) the Fe(II)–Fe(III) solid-phase redox product of Tc(VII)–Fe(II) homogeneous reaction (Zachara et al., 2007). The Fe(II)-ferrihydrite in these latter two systems, despite higher Fe(II) content, displayed only broad sextets at 77 K unlike the distinct Fe(II) doublet noted in the present samples at $\geqslant$77 K (Fig. 6B and C).

It was not possible from Mössbauer spectroscopy to determine whether sorbed Fe(II) resulting from AH_2DS reaction in the presence of P was adsorbed to or precipitated with ferrihydrite, or present as a separate phase. Perhaps the distinction between surface complexes and structural incorporation is insignificant given the disordered ferrihydrite structure (Michel et al., 2007). We did not observe an octet pattern for sorbed Fe(II) at 10 K. This Mössbauer feature was reported for surface-associated Fe(II) on hematite above site saturation, and was attributed to a $Fe(OH)_2$-like phase (Larese-Casanova and Scherer, 2007). The observed Mössbauer parameters of Fe(III) and Fe(II) in the +P sample, and their temperature dependence, implied that the reacted mineral residue retained the starting ferrihydrite structure with sorbed Fe(II) in highly distorted environments. The minor differences in the ferrihydrite features resulted from the formation of 6-line from 2-line ferrihydrite (Figs. 4 and 6).

The reductive mineralization of ferrihydrite at $Fe(II)_{equiv}/Fe(III) = 0.54$ in the AH_2DS system, where sorbed Fe(II) was ~33% of Fe_{total}, was similar in both +P and −P systems. Stoichiometric magnetite was the only product (Fig. 8). There were no hints of green rust, lepidocrocite, or any other precursor in the 77-K Mössbauer spectrum (not shown). The presence of incipient peaks due to magnetite in the 1 d samples implied solid-state conversion induced by Fe(II) sorption and electron transfer to structural Fe(III) (Cornell, 1988; Mann and Frankel, 1989; Tronc et al., 1992). The morphology of the magnetite was different from those created by dissolution/precipitation (Vali et al., 2004; Behrends and Van Cappellen, 2007). Sorbed P had no apparent influence on this AH_2DS-mediated solid-state reaction that was different from the proposed Fe(II)-rich ferrihydrite to lepidocrocite to magnetite pathway of the aqueous Fe(II)-ferrihydrite system (Hansel et al., 2005). Perhaps higher interfacial pH promoted by AH_2DS oxidation facilitated P desorption.

The presence of P inhibited 2-line Si-ferrihydrite transformation to lepidocrocite in PIPES buffer over a 1 d reaction period at all studied concentrations of $Fe(II)_{aq}$ (Fig. 11 and EA-6). However, this inhibition was relieved over time as comparable amounts of lepidocrocite were observed in the +P and −P systems after 30 d (Figs. 10 and 11). These concentrations did not change after an additional 33 d of equilibration (to 63 d, Fig. EA-5). The initial inhibition did not result from any change in Fe(II) solid–liquid distribution (i.e., electron transfer) as $Fe(II)_{aq}$ concentrations were insensitive to the presence of P (Fig. 9). In contrast to the AH_2DS system, the presence of P strongly inhibited magnetite formation by $Fe(II)_{aq}$. A comparable observation was made by Borch et al. (2007). System pH may have been a factor in our experiments as a lower pH in the $Fe(II)_{aq}$ system may have both strengthened P surface complexation, and lowered the magnetite formation rate. This apparent inhibition did not diminish even after 63 d of incubation. Adsorbed P may hinder reductive mineralization by blocking condensation sites at the nm scale necessary for formation of long-range order.

An unresolved issue in the current study is the fate of Si that was coprecipitated with ferrihydrite. We have noted in previous studies that the coprecipitated Si is labile and responsive to P concentration. Si changes in solid–liquid distribution during ferrihydrite phase transformations (Kukkadapu et al., 2004). It is also not conservative once released to the aqueous phase and may substitute to limited degrees in reductive transformation products (Glasauer

et al., 1999; Schwertmann et al., 2004), and adsorb to their surfaces (Eick et al., 2009). The trajectory of aqueous and ferrihydrite-sorbed Si during the course of the present experiments is not known. Is it possible for desorbed Si to further enrich Si in the residual ferrihydrite to levels that impact its subsequent reactivity with Fe(II)? The behavior of Si should be considered in future experiments given the recent results of Jones et al. (2009).

4.3. Implications to MRB–AQDS–ferrihydrite systems

When AQDS is used as a ETM with MRB, an electron donor, and ferrihydrite/or lepidocrocite, it is generally present at lower concentration with a $Fe(II)_{equiv}$/Fe(III) ratio ranging from approximately 0.0004 (Zegeye et al., 2007; Coker et al., 2008) to 0.0072 (Fredrickson et al., 1998; Kukkadapu et al., 2004). Consequently, the heterogeneous reductant (AH_2DS) is supplied at a low, but more sustained and uniform concentration than in the present experiments as a result of bacterial respiration. The system is flux-, rather than concentration-driven. The total electron equivalents delivered to the solid are a complex function of the electron donor concentration, respiration rate (organism density), and AQDS concentration (Zegeye et al., 2007; O'Loughlin, 2008); and not the total concentration of AQDS as observed here.

Comparisons between +AQDS and -AQDS systems suggest that the primary role of AQDS is to enhance reduction/mineralization kinetics, reaction product crystallization, and the dispersal of electron equivalents to less accessible domains, e.g., within aggregates or mineral surfaces not in cell contact (Fredrickson et al., 1998; Zachara et al., 1998; Coker et al. 2008; Zegeye et al., 2007; Cutting et al., 2009). The presence of AQDS may also reduce the temporal stability of mineralogic intermediates (Coker et al., 2008). Consistent with the results of this study, the presence of AQDS enhanced magnetite formation by MRB from both ferrihydrite and lepidocrocite (Cutting et al., 2009). While these authors attributed their observations to enhanced Fe(II) flux mediated by AQDS, it is more probable that this was a direct AQDS effect as observed herein. Uncertain is the role of interfacial pH on reductive mineralization as influenced by heterogeneous AH_2DS oxidation, either as a temporal excursion or sustained condition.

The long-term persistence of lepidocrocite in our $Fe(II)_{aq}$ system (e.g., 63 d, Fig. 10), contrasted with its transformation by MRB under comparable or shorter time periods (Vali et al., 2004; Cutting et al., 2009; O'Loughlin et al., 2010). Consistent with our findings, both Pedersen et al. (2005) and Hansel et al. (2005) also noted little transformation of lepidocrocite to magnetite by $Fe(II)_{aq}$ in the absence of MRB activity. Magnetite, in contrast, was an important bioreduction product of lepidocrocite by: (i) *Geobacter sulfurreducens* in bicarbonate buffer after 6 d (Cutting et al., 2009), that was enhanced by AQDS presence, and (ii) *Shewanella putrefaciens* in presence of AQDS in unbuffered media after 50 d (O'Loughlin et al., 2010). Vali et al. (2004) observed the formation of lepidocrocite from ferrihydrite in 6.25 d using *Geobacter metallireducens* in PIPES buffer, and its subsequent complete transformation to tabular, single domain magnetite in 27.8 d. Our results, however, showed that an elevated $Fe(II)_{aq}$ concentration and favorable pH, as well as aqueous chemical conditions in the magnetite stability range, are alone insufficient to induce lepidocrocite transformation to magnetite over 63 d. These noted differences may result from crystallite size/reactivity effects (our recrystallized lepidocrocite was relatively large in size, Fig. 12) or a potentially active, direct role of MRB in the lepidocrocite to magnetite transformation.

Green rust is a reductive mineralization product in MRB–AQDS–ferrihydrite (Fredrickson et al., 1998; Kukkadapu et al., 2004) and lepidocrocite systems (O'Loughlin et al., 2007, 2010; Zegeye et al., 2007; O'Loughlin, 2008). While green rust has been observed without AQDS (Ona-Nguema et al., 2002; Zegeye et al., 2007); the ETM has been a common component of media in which significant green rust has formed. Important differences exist between these studies in media composition including P and C; cell concentrations influencing aggregation state and respiration rate [e.g., Fe(II) and bicarbonate flux]; Fe(III) oxide preparation method and crystallite size, storage history, and concentration; buffer use and concentration; and other experimental variables. Consequently, the identification of common mineral transformation pathways and the distinctive role of AQDS is difficult. Moreover, green rust is not always the final mineral product formed; and, for both ferrihydrite and lepidocrocite, specific conditions seem to be required, e.g., the presence of P (Bocher et al., 2004; Kukkadapu et al., 2004). For lepidocrocite specifically, high cell concentrations that promote as yet undefined aggregation effects appear necessary for green rust formation (Zegeye et al., 2007). Beyond this, it is perhaps significant that green rust is most frequently observed in un-buffered systems where pH increases to values over 8 in consequence to iron reduction.

Green rust formation did not occur in our experiments with AH_2DS regardless of reactant ratio. Consequently, green rust appears to be a biogenic phase in certain settings controlled by unique combinations of experimental variables. Whether these conditions can be achieved in natural biogeochemical environments with significant natural pH buffering capacity, and in the absence of a low redox potential ETM such as AQDS is uncertain. Also uncertain is whether natural ETM, including humic substances (e.g., Nurmi and Tratnyek, 2002; Jiang and Kappler, 2008) and biogenic flavins (Marsili et al., 2008; Von Canstein et al., 2008; Ross et al., 2009) can function equally or even significantly in this regard.

5. CONCLUSIONS

Ferrihydrite is one of the most important Fe(III) oxides in subsurface environments because of its common occurrence and high reactivity. The findings presented herein complement other recent investigations on the reductive transformations of ferrihydrite. While there is general consensus on the nature of reductive transformation products and some of the conditions that promote them (e.g., this pa-

per, Hansel et al., 2005; Borch et al., 2007; Coker et al., 2008), there is disagreement on pathways, the presence or absence of intermediate or precursor phases, kinetic relationships, and transformation mechanisms. To large degree, these disagreements result from: (i) the large number of important influential (bio)geochemical variables and their relevant ranges (e.g., pH, Fe(II) concentration, ferrihydrite concentration and nature, carbonate concentration, presence or absence of Si, presence or absence of ETM; etc.) and the inability to control or vary them in a suitably robust manner, and (ii) experimental differences and analytical methods. A truly integrative conceptual model of ferrihydrite reductive transformation in absence and presence of MRB will require precise control of key geochemical parameters over a large multi-dimensional domain, innovative experimentation, and application of multiple complementary analytical methods over critical timescales.

ACKNOWLEDGMENTS

This research was supported by the Geosciences Research Program of the Office of Basic Energy Science (BES), US Department of Energy (DOE). X-ray diffraction (XRD), electron microscopy, and Mössbauer measurements were performed using EMSL, a national scientific user facility sponsored by the Department of Energy's Office of Biological and Environmental Research and located at Pacific Northwest National Laboratory. PNNL is operated for the Department of Energy by Battelle. We acknowledge the assistance of Janae Strickland, Colleen Russell, and Odeta Qafoku with experimentation, XRD, and Mössbauer measurements. Appreciated comments and recommendations were provided by three anonymous reviewers that improved the manuscript.

APPENDIX A. SUPPLEMENTARY DATA

Supplementary data associated with this article can be found, in the online version, at doi:10.1016/j.gca.2011.06.030.

REFERENCES

Anderson P. R. and Benjamin M. M. (1985) Effect of silicon on the crystallization and adsorption properties of ferric oxides. *Environ. Sci. Technol.* **19**, 1048–1053.

Arai Y. and Sparks D. L. (2001) ATR-FTIR spectroscopic investigation on phosphate adsorption mechanisms at the ferrihydrite–water interface. *J. Colloid Interface Sci.* **241**, 317–326.

Baedecker M. J., Cozzarelli I. M., Eganhouse R. P., Siegel D. I. and Bennett P. C. (1993) Crude oil in a shallow sand and gravel aquifer – III. Biogeochemical reactions and mass balance modeling in anoxic groundwater. *Appl. Geochem.* **8**, 569–586.

Banfield J. F., Welch S. A., Zhang H., Ebert T. T. and Penn R. L. (2000) Aggregation-based crystal growth and microstructure development in natural iron oxyhydroxide biomineralization products. *Science* **289**, 751–754.

Behrends T. and Van Cappellen P. (2007) Transformation of hematite into magnetite during dissimilatory iron reduction – conditions and mechanisms. *Geomicrobiol. J.* **24**, 403–416.

Bennett P. C., Siegel D. E., Baedecker M. J. and Hult M. F. (1993) Crude oil in a shallow sand and gravel aquifer – I. Hydrogeology and inorganic geochemistry. *Appl. Geochem.* **8**, 529–549.

Bhushan B., Halasz A. and Hawari J. (2006) Effect of iron(III), humic acids, and anthraquinone-2,6-disulfonate on biodegradation of cyclic nitromines by *Clostridium* sp. EDB2. *J. Appl. Microbiol.* **100**, 555–563.

Biber M. V., Dos Santos Afonso M. and Stumm W. (1994) The coordination chemistry of weathering: IV. Inhibition of the dissolution of oxide minerals. *Geochim. Cosmochim. Acta* **58**, 1999–2010.

Bocher F., Gehin A., Ruby C., Ghanbaja J., Abdelmoula M. and Genin J.-M. R. (2004) Coprecipitation of Fe(II–III) hydroxycarbonate green rust stabilized by phosphate adsorption. *Solid State Sci.* **6**, 117–124.

Bonneville S., Van Cappellen P. and Behrends T. (2004) Microbial reduction of iron(III) oxyhydroxides: effects of mineral solubility and availability. *Chem. Geol.* **212**, 255–268.

Borch T., Inskeep W. P., Harwood J. A. and Gerlach R. (2005) Impact of ferrihydrite and anthraquinone-2,6-disulfonate on the reductive transformation of 2,4,6-trinitrotoluene by a gram-positive fermenting bacterium. *Environ. Sci. Technol.* **39**, 7126–7133.

Borch T., Masue Y., Kukkadapu R. K. and Fendorf S. (2007) Phosphate imposed limitations on biological reduction and alteration of ferrihydrite. *Environ. Sci. Technol.* **41**, 166–172.

Burgos W. D., Fang Y. L., Royer R. A., Yeh G. T., Stone J. J., Jeon B. H. and Dempsey B. A. (2003) Reaction-based modeling of quinone-mediated bacterial iron(III) reduction. *Geochim. Cosmochim. Acta* **67**, 2735–2748.

Carlson L. and Schwertmann U. (1981) Natural ferrihydrites in surface deposits from Finland and their association with silica. *Geochim. Cosmochim. Acta* **45**, 421–429.

Carlson L. and Schwertmann U. (1990) The effect of CO_2 and oxidation rate on the formation of goethite versus lepidocrocite from a Fe(II) system at pH 6 and 7. *Clay Miner.* **25**, 65–71.

Chacon N., Silver W. L., Dubinsky E. A. and Cusack D. F. (2006) Iron reduction and soil phosphorus solubilization in humid tropical forests soils: the roles of labile carbon pools and an electron shuttle compound. *Biogeochemistry* **78**, 67–84.

Coker V. S., Bell A. M. T., Pearce C. I., Pattrick R. A. D., Van Der Laan G. and Lloyd J. R. (2008) Time-resolved synchrotron powder X-ray diffraction study of magnetite formation by the Fe(III)-reducing bacterium *Geobacter sulfurreducens*. *Am. Mineral.* **93**, 540–547.

Cornell R. M. (1988) The influence of some divalent cations on the transformation of ferrihydrite into more crystalline products. *Clay Miner.* **23**, 329–332.

Cornell R. M. and Giovanoli R. (1987) The influence of silicate species on the morphology of goethite (α-FeOOH) grown from ferrihydrite ($5Fe_2O_3{\cdot}9H_2O$). *JCS Chem. Commun.*, 413–414.

Cornell R. M., Giovanoli R. and Schindler P. W. (1987) Effect of silicate species on the transformation of ferrihydrite into goethite and hematite in alkaline media. *Clays Clay Miner.* **35**, 21–28.

Cornell R. M., Giovanoli R. and Schneider W. (1989a) The transformation of ferrihydrite into lepidocrocite. *Clay Miner.* **24**, 549–553.

Cornell R. M., Schneider W. and Giovanoli R. (1989b) Phase transformation in the ferrihydrite/cysteine system. *Polyhedron* **8**, 2829–2834.

Cornell R. M. and Schwertmann U. (2003) *The Iron Oxides: Structure, Reactions, Occurrences and Uses*, 2nd ed. Wiley-VCH.

Curtis G. P. and Reinhard M. (1994) Reductive dehalogenation of hexachlorethane, carbon-tetrachloride, and bromoform by anthrahydroquinone disulfonate and humic-acid. *Environ. Sci. Technol.* **28**, 2392–2401.

Cutting R. S., Coker V. S., Fellowes J. W., Lloyd J. R. and Vaughan D. J. (2009) Mineralogical and morphological constraints on the reduction of Fe(III) minerals by *Geobacter sulfurrenducens*. *Geochim. Cosmochim. Acta* **73**, 4004–4022.

DiChristina T. J., Fredrickson J. K. and Zachara J. M. (2005) Enzymology of electron transport: energy generation with geochemical consequences. In *Reviews in Mineralogy & Geochemistry*, vol. 59 (eds. J. F. Banfield, J. Cervini-Silva and K. M. Nealson). Mineralogical Society of America, pp. 27–52.

Dong H. L., Kostka J. E. and Kim J. (2003) Microscopic evidence for microbial dissolution of smectite. *Clays Clay Miner.* **51**, 502–512.

Dyer L., Fawell P. D., Newman O. M. G. and Richmond W. R. (2010) Synethsis and characterization of ferrihydrite/silica co-precipitates. *J. Colloid Interface Sci.* **348**, 65–70.

Dzombak D. A. and Morel F. M. M. (1990) *Surface Complexation Modeling-Hydrous Ferric Oxide*. John Wiley & Sons, New York, NY.

Eick M. J., Luxton T. P. and Welsh H. A. (2009) Effect of silica polymerization on the oxalate-promoted dissolution of goethite. *Clays Clay Miner.* **57**, 578–585.

Faivre D., Agrinier P., Menguy N., Zuddas P., Pachana K., Gloter A., Laval J-. Y. and Guyot F. (2004) Mineralogical and isotopic properties of inorganic nanocrystalline magnetites. *Geochim. Cosmochim. Acta* **68**, 4395–4403.

Fortin D., Leppard G. G. and Tessier A. (1993) Characteristics of lacustrine diagenetic iron oxyhydroxides. *Geochim. Cosmochim. Acta* **57**, 4391–4404.

Fredrickson J. K., Zachara J. M., Kennedy D. W., Dong H., Onstott T. C., Hinman N. W. and Li S. W. (1998) Biogenic iron mineralization accompanying the dissimilatory reduction of hydrous ferric oxide by a ground water bacterium. *Geochim. Cosmochim. Acta* **62**, 3239–3257.

Fredrickson J. K., Zachara J. M., Kennedy D. W., Kukkadapu R. K., McKinley J. P., Heald S. M., Liu C., Plymale A. E. and Smith S. C. (2004) Reduction of TcO_4^- by sediment-associated biogenic Fe(II). *Geochim. Cosmochim. Acta* **68**, 3171–3187.

Galvez N., Barron V. and Torrent J. (1999) Effect of phosphate on the crystallization of hematite, goethite, and lepidocrocite from ferrihydrite. *Clays Clay Miner.* **47**, 304–311.

Geomicrobiology, (2002) Microbial Fe(III) oxide reduction. In *An International Journal of Geomicrobiology and Microbial Biogeochemistry* (eds. E. E. Roden and Y. A. Gorby), vol. 19. Taylor & Francis, London, UK.

Glasauer S., Friedl J. and Schwertmann U. (1999) Properties of goethites prepared under acidic and basic conditions in the presence of silicate. *J. Colloid Interface Sci.* **216**, 106–115.

Greenwood N. N. and Gibb T. C. (1971) *Mössbauer Spectroscopy*. Chapman and Hall, London.

Hansel C. M., Benner S. G., Neiss J., Dohnalkova A., Kukkadapu R. K. and Fendorf S. (2003) Secondary mineralization pathways induced by dissimilatory iron reduction of ferrihydrite under advective flow. *Geochim. Cosmochim. Acta* **67**, 2977–2992.

Hansel C. M., Benner S. G. and Fendorf S. (2005) Competing Fe(II)-induced mineralization pathways of ferrihydrite. *Environ. Sci. Technol.* **39**, 7147–7153.

Hernandez M. E., Kappler A. and Newman D. K. (2004) Phenazines and other redox-active antibiotics promote microbial mineral reduction. *Appl. Environ. Microbiol.* **70**, 921–928.

Jaisi D. P., Dong H. and Liu C. (2007) Influence of biogenic Fe(II) on the extent of microbial reduction of Fe(III) in clay minerals nontronite, illite, and chlorite. *Geochim. Cosmochim. Acta* **71**, 1145–1158.

Jiang J. and Kappler A. (2008) Kinetics of microbial and chemical reduction of humic substances: implications for electron shuttling. *Environ. Sci. Technol.* **42**, 3563–3569.

Jones A. M., Collins R. N., Rose J. and Waite T. D. (2009) The effect of silica and natural organic matter on the Fe(II)-catalyzed transformation and reactivity of Fe(III) minerals. *Geochim. Cosmochim. Acta* **72**, 4409–4422.

Jones D. P., Y-Mi Go., Anderson C. L., Ziegler T. R., Kinkade J. M. and Kirlin W. (2004) Cysteine/cystine couple is a newly recognized node in the circuitry for biologic redox signaling and control. *FASEB J.* **18**, 1246–1248.

Jones D. P., Fennessey C. M., DiChristina T. J. and Taillefert M. (2010) *Shewanella oneidensis* MR-1 mutants selected for their inability to produce soluble organic-Fe(III) complexes are unable to respire Fe(III) as anaerobic electron acceptor. *Environ. Microbiol.* **12**, 938–950.

Kappler A. and Straub K. L. (2005) Geomicrobiological cycling of iron. *Mol. Geomicrobiol.* **59**, 85–108.

Khare N., Martin J. D. and Hesterberg D. (2007) Phosphate bonding configuration of ferrihydrite based on molecular orbital calculations and XANES fingerprinting. *Geochim. Cosmochim. Acta* **71**, 4404–4415.

Komlos J., Kukkadapu R. K., Zachara J. M. and Jaffe P. R. (2007) Biostimulation of iron reduction and subsequent oxidation of sediment containing Fe-silicates and Fe-oxides: effect of redox cycling on Fe(III) bioreduction. *Water Res.* **41**, 2996–3004.

Kostka J. E., Dalton D. D., Skelton H., Dollhopf S. and Stucki J. W. (2002) Growth of iron(III)-reducing bacteria on clay minerals as the sole electron acceptor and comparison of growth yields on a variety of oxidized iron forms. *Appl. Environ. Microbiol.* **68**, 6256–6262.

Kukkadapu R. K., Zachara J. M., Fredrickson J. K., Smith S. C., Dohnalkova A. C. and Russell G. K. (2003) Transformation of 2-line ferrihydrite to 6-line ferrihydrite under oxic and anoxic conditions. *Am. Mineral.* **88**, 1903–1914.

Kukkadapu R. K., Zachara J. M., Fredrickson J. K. and Kennedy D. W. (2004) Biotransformation of synthetic 2-line silica-ferrihydrite coprecipitates by a dissimilatory Fe(III)-reducing bacterium: formation of carbonate green rust in the presence of phosphate. *Geochim. Cosmochim. Acta* **68**, 2799–2814.

Kukkadapu R. K., Zachara J. M., Fredrickson J. K., Kennedy D. W., Dohnalkova A. C. and McCready D. E. (2005) Ferrous hydroxy carbonate is a stable transformation product of biogenic magnetite. *Am. Mineral.* **90**, 510–515.

Kukkadapu R. K., Zachara J. M., Fredrickson J. K., McKinley J. P., Kennedy D. W., Smith S. C. and Dong H. (2006) Reductive biotransformation of Fe in shale-limestone saprolite containing Fe(III) oxides and Fe(II)/Fe(III) phyllosilicates. *Geochim. Cosmochim. Acta* **70**, 3662–3676.

Kwon M. J. and Finneran K. T. (2006) Microbially mediated biodegradation of hexahydro-1,3,5-trinitro-1,3,5-triazine by extracellular electron shuttling compounds. *Appl. Environ. Microbiol.* **72**, 5933–5941.

Kwon M. J. and Finneran K. T. (2008) Biotransformation products and mineralization potential for hexahydro-1,3,5-trinitro-1,3,5-triazine (RDX) in abiotic versus biological degradation pathways with anthraquinone-2,6-disulfonate (AQDS) and *Geobacter metallireducens*. *Biodegradation* **19**, 705–715.

Larese-Casanova P. and Scherer M. M. (2007) Fe(II) sorption on hematite: new insights based on spectroscopic measurements. *Environ. Sci. Technol.* **41**, 471–477.

Liu C., Zachara J. M., Foster N. S. and Strickland J. (2007a) Kinetics of reductive dissolution of hematite by bioreduced anthraquinone-2,6-difulfonate. *Environ. Sci. Technol.* **41**, 7730–7735.

Liu H., Li P., Zhu M. Y., Wei Y. and Sun Y. H. (2007b) Fe(II)-induced transformation from ferrihydrite to lepidocrocite and goethite. *J. Solid State Chem.* **180**, 2121–2128.

Lovley D. R. and Anderson R. T. (2000) Influence of dissimilatory metal reduction on the fate of organic and metal contaminants in the subsurface. *Hydrogeol. J.* **8**, 77–88.

Majzlan J. (2008) Stabilization of iron oxide nanoparticles by the adsorption of sulfate, phosphate and arsenate. *Geochim. Cosmochim. Acta* **72**(12), A587.

Mann S. and Frankel R. B. (1989) Magnetite biomineralization in unicellular microorganisms. In *Biomineralization: Chemical and Biochemical Perspectives* (eds. S. Mann, J. Webb and R. J. P. Williams). VCH, Weinheim, pp. 389–426.

Mann S., Sparks N. H. C., Couling S. B., Larcombe M. C. and Frankel R. B. (1989) Crystallochemical characterization of magnetic spinels prepared from aqueous solution. *J. Chem. Soc. Faraday Trans. I* **85**, 3033–3044.

Marsili E., Baron D. B., Shikhare I. D., Coursolle D., Gralnick J. A. and Bond D. R. (2008) *Shewanella* secretes flavins that mediate extracellular electron transfer. *PNAS* **105**, 3968–3973.

Mehta T., Coppi M. V., Childers S. E. and Lovley D. R. (2005) Outer membrane c-type cytochromes required for Fe(III) and Mn(IV) oxide reduction in *Geobacter sulfurreducens*. *Appl. Environ. Microbiol.* **71**, 8634–8641.

Michel F. M., Ehm L., Antao S. M., Lee P. L., Chupas P. J., Liu G., Strongin D. R., Schoonen M. A. A., Phillips B. L. and Parise J. B. (2007) The structure of ferrihydrite, a nanocrystalline material. *Science* **316**, 1726–1729.

Murad E. and Cashion J. (2004) *Mössbauer Spectroscopy of Environmental Materials and Their Industrial Utilization*. Kluwer Academic Publishers, Boston/Dordrecht/ New York/ London.

Nevin K. P. and Lovley D. R. (2000a) Lack of production of electron-shuttling compounds or solubilization of Fe(III) during reduction of insoluble Fe(III) oxide by *Geobacter metallireducens*. *Appl. Environ. Microbiol.* **66**, 2248–2251.

Nevin K. P. and Lovley D. R. (2000b) Potential for nonenzymatic reduction of Fe(III) via electron shuttling in subsurface sediments. *Environ. Sci. Technol.* **34**, 2472–2478.

Nurmi J. T. and Tratnyek P. G. (2002) Electrochemical properties of natural organic matter (NOM), fractions of NOM, and model biogeochemical electron shuttles. *Environ. Sci. Technol.* **36**, 617–624.

O'Loughlin E. J., Larese-Casanova P., Scherer M. and Cook R. (2007) Green rust formation from the bioreduction of γ-FeOOH (lepidocrocite): comparison of several *Shewanella* species. *Geomicrobiol. J.* **24**, 211–230.

O'Loughlin E. J. (2008) Effects of electron transfer mediators on the bioreduction of lepidocrocite (γ-FeOOH) by *Shewanella putrefaciens* CN32. *Environ. Sci. Technol.* **42**, 6876–6882.

O'Loughlin E. J., Gorski C. A., Scherer M. M., Boyanov M. I. and Kemner K. M. (2010) Effects of oxyanions, natural organic matter, and bacterial cell numbers on the bioreduction of lepidocrocite (γ-FeOOH) and the formation of secondary mineralization products. *Environ. Sci. Technol.* **44**, 4570–4576.

Ona-Nguema G., Abdelmoula M., Jorand F., Benali O., Géhin A., Block J.-C. and Génin J. M. R. (2002) Iron (II, III) hydroxycarbonate green rust formation and stabilization from lepidocrocite bioreduction. *Geochim. Cosmochim. Acta* **36**, 16–20.

Pedersen H. D., Postma D., Jakobsen R. and Larsen O. (2005) Fast transformation of iron oxyhydroxides by the catalytic action of aqueous Fe(II). *Geochim. Cosmochim. Acta* **69**, 3967–3977.

Perret D., Gaillard J. F., Dominik J. and Atteia O. (2000) The diversity of hydrous iron oxides. *Environ. Sci. Technol.* **34**, 3540–3546.

Plymale A. E., Fredrickson J. K., Zachara J. M., Dohnalkova A. C., Heald S. M., Moore D. A., Kennedy D. W., Marshall M. J., Wang C. and Nachimuthu P. (2011) Competitive reduction of pertechnetate ($^{99}TcO_4^-$) by dissimilatory metal reducing bacteria and biogenic Fe(II). *Environ. Sci. Technol.* **45**, 951–957.

Rancourt D. G. and Ping J. Y. (1991) Voigt-based methods for arbitrary-shape static hyperfine parameter distributions in Mössbauer spectroscopy. *Nucl. Instrum. Methods Phys. Rev.* **B58**, 85–87.

Roden E. E. and Zachara J. M. (1996) Microbial reduction of crystalline Fe(III) oxides: influence of oxide surface area and potential for cell growth. *Environ. Sci. Technol.* **30**, 1618–1628.

Roden E. E. (2006) Geochemical and microbiological controls on dissimilatory iron reduction. *C. R. Geosci.* **338**, 456–467.

Ross D. E., Brantley S. L. and Tien M. (2009) Kinetic characterization of OmcA and MtrC, terminal reductases involved in respiratory electron transfer for dissimilatory iron reduction in *Shewanella oneidensis* MR-1. *Appl. Environ. Microbiol.* **75**, 5218–5226.

Royer R. A., Burgos W. D., Fisher A. S., Jeon B. H., Unz R. F. and Dempsey B. A. (2002) Enhancement of hematite bioreduction by natural organic matter. *Environ. Sci. Technol.* **36**, 2897–2904.

Schwertmann U. and Thalmann H. (1976) The influence of [Fe(II)], [Si], and pH on the formation of lepidocrocite and ferrihydrite during oxidations of aqueous $FeCl_2$ solutions. *Clay Miner.* **11**, 189–200.

Schwertmann U. and Cornell R. M. (2000) *Iron Oxides in the Laboratory*. Wiley-VCH, Weiheim, Germany.

Schwertmann U., Friedel J. and Kyek A. (2004) Formation and properties of a continuous crystallinity series of synthetic ferrihydrites (2- to 6-line) and their relation to FeOOH forms. *Clays Clay Miner.* **52**, 221–226.

Shi L., Squier T. C., Zachara J. M. and Fredrickson J. K. (2007) Respiration of metal (hydr)oxides by *Shewanella* and *Geobacter*: a key role for multihaem c-type cytochromes. *Mol. Microbiol.* **65**, 12–20.

Shyu J. B. H., Lies D. P. and Newman D. K. (2002) Protective role of tolC in efflux of the electron shuttle anthraquinone-2,6-disulfonate. *J. Bacteriol.* **184**, 1806–1810.

Straub K. L. and Schink B. (2003) Evaluation of electron-shuttling compounds in microbial ferric iron reduction. *FEMS Microbiol. Lett.* **220**, 229–233.

Stookey L. L. (1970) Ferrozine – A new spectrophotometric reagent for iron. *Anal. Chem.* **42**, 779–781.

Swedlund P. J., Miskelly G. M. and McQuillan A. J. (2009) An attenuated total reflectance IR study of silicic acid adsorbed onto a ferric oxyhydroxide surface. *Geochim. Cosmochim. Acta* **73**, 4199–4214.

Taillefert M., Beckler J. S., Carey E., Burns J. L., Fennessey C. M. and DiChristina T. J. (2007) *Shewanella putrefaciens* produces an Fe(III)-solubilizing organic ligand during anaerobic respiration on insoluble Fe(III) oxides. *J. Inorg. Biochem.* **101**, 1760–1767.

Tessier A., Fortin D., Belzile N., DeVitre R. R. and Leppard G. (1996) Metal sorption to diagenetic iron and manganese oxyhydroxides and associated organic matter: aarrowing the gap between field and laboratory measurements. *Geochim. Cosmochim. Acta* **60**, 387–404.

Tronc E., Belleville P., Jolivet J.-P. and Livage J. (1992) Transformation of ferric hydroxide into spinel by Fe(II) adsorption. *Langmuir* **8**, 313–319.

Vali H., Weiss B., Li Y. L., Sears S. K., Kim S. S., Kirschvink J. L. and Zhang C. L. (2004) Formation of tabular single-domain magnetite induced by *Geobacter metallireducens* GS-15. *PNAS* **101**, 16121–16126.

von Canstein H., Ogawa J., Shimizu S. and Lloyd J. R. (2008) Secretion of flavins by *Shewanella* species and their role in extracellular electron transfer. *Appl. Environ. Microbiol.* **74**, 615–623.

Voordeckers J. W., Kim B. C., Izallalen M. and Lovley D. R. (2010) Role of *Geobacter sulfurreducens* outer surface c-type cytochromes in reduction of soil humic acid and anthraquinone-2,6-disulfonate. *Appl. Environ. Microbiol.* **76**, 2371–2375.

Weber K. A., Achenbach L. A. and Coates J. D. (2006) Microorganisms pumping iron: anaerobic microbial iron oxidation and reduction. *Nat. Rev. Microbiol.* **4**, 752–764.

Xu Y. and Axe L. (2005) Synthesis and characterization of iron oxide-coated silica and its effect on metal adsorption. *J. Colloid Interface Sci.* **282**, 11–19.

Yan B., Wrenn B. A., Basak S., Biswas P. and Giammar D. E. (2008) Microbial reduction of Fe(III) in hematite nanoparticles by *Geobacter sulfurreducens*. *Environ. Sci. Technol.* **42**, 6526–6531.

Zachara J. M., Fredrickson J. K., Li S. W., Kennedy D. W., Smith S. C. and Gassman P. L. (1998) Bacterial reduction of crystalline Fe(III) oxides in single phase suspensions and subsurface materials. *Am. Mineral.* **83**, 1426–1443.

Zachara J. M., Kukkadapu R. K., Fredrickson J. K., Gorby Y. A. and Smith S. C. (2002) Biomineralization of poorly crystalline Fe(III) oxides by dissimilatory metal reducing bacteria (DMRB). *Geomicrobiol. J.* **19**, 179–207.

Zachara J. M., Kukkadapu R. K., Gassman P. L., Dohnalkova A., Fredrickson J. K. and Anderson T. (2004) Biogeochemical transformation of Fe minerals in a petroleum-contaminated aquifer. *Geochim. Cosmochim. Acta* **68**, 1791–1805.

Zachara J. M., Heald S. M., Jeon B.-H., Kukkadapu R. K., Liu C., McKinley J. P., Dohnalkova A. C. and Moore D. (2007) Reduction of pertechnetate [Tc(VII)] by aqueous Fe(II) and the nature of solid phase redox products. *Geochim. Cosmochim. Acta* **71**, 2137–2157.

Zegeye A., Ruby C. and Jorand F. (2007) Kinetic and thermodynamic analysis during dissimilatory γ-FeOOH reduction: formation of green rust 1 and magnetite. *Geomicrobiol. J.* **24**, 51–64.

Zhang Y. Q., Zahir Z. A., Amrhein C., Chang A. and Frankenberger W. T. (2007) Application of redox mediator to accelerate selenate reduction to elemental selenium by *Enterobacter taylorae*. *J. Agric. Food Chem.* **55**, 5714–5717.

Zhao J., Huggins F. E., Feng Z. and Huffman G. P. (1996) Surface-induced superparamagnetic relaxation in nanoscale ferrihydrite particles. *Phys. Rev. B* **54**, 3403–3407.

Associate editor: Donald L. Sparks